Structural basis for small molecule targeting of Doublecortin Like Kinase 1 DCLK1

Onisha Patel
The Walter and Eliza Hall Institute of Medical Research
Michael Roy
The Walter and Eliza Hall Institute of Medical Research https://orcid.org/0000-0003-0198-9108
Ashleigh Kropp
The Walter and Eliza Hall Institute of Medical Research
Weiwen Dai
The Walter and Eliza Hall Institute of Medical Research
Isabelle Lucet (lucet.i@wehi.edu.au)
The Walter and Eliza Hall Institute of Medical Research https://orcid.org/0000-0002-8563-8753

Article

Keywords: Doublecortin Like Kinase 1, Microtubule Associated Protein, Scaffolds, Cell signalling, Cancer, kinase inhibitors

Posted Date: January 15th, 2021

DOI: https://doi.org/10.21203/rs.3.rs-133153/v1

Version of Record: A version of this preprint was published at Communications Biology on September 20th, 2021. See the published version at https://doi.org/10.1038/s42003-021-02631-y.

Structural basis for small molecule targeting of Doublecortin Like Kinase 1 DCLK1

Onisha Patel[1,2,*], Michael Roy[1,2], Ashleigh Kropp[1,2], Weiwen Dai[1,2] and Isabelle Lucet[1,2,*]

1. The Walter and Eliza Hall Institute of Medical Research, Parkville, Victoria 3052, Australia
2. Department of Medical Biology, University of Melbourne, Parkville, Victoria, 3052.

[*]Correspondence: lucet.i@wehi.edu.au, patel.o@wehi.edu.au

Lead contact: lucet.i@wehi.edu.au

Keywords: Doublecortin Like Kinase 1, Microtubule Associated Protein, Scaffolds, Cell signalling, Cancer, kinase inhibitors

Running title: Structural basis for DCLK1-IN-1 inhibition

Abstract

Doublecortin-like kinase 1 (DCLK1) is a bi-functional protein classified as a Microtubule-Associated Protein (MAP) and as a serine/threonine kinase that plays a critical role in regulating microtubule assembly. This understudied kinase is upregulated or mutated in a wide range of cancers. Knockdown studies have shown that DCLK1 is functionally important for tumour growth. However, the presence of tissue and development specific spliced DCLK1 isoforms and the lack of systematic evaluation of their biological function have challenged the development of effective strategies to understand the role of DCLK1 in oncogenesis. Recently, DCLK1-IN-1 was reported as a potent and selective DCLK1 kinase inhibitor, a powerful new tool to dissect DCLK1 biological functions.

Here, we report the crystal structures of DCLK1 kinase domain in complex with two DCLK1-IN-1 precursors and DCLK-IN-1. Combined, our structural data analysis illuminates and rationalises the structure-activity relationship that informed development of DCLK1-IN-1 and provides the basis for DCLK1-IN-1 increased selectivity. We show that DCLK1-IN-1 induces a drastic conformational change of the N-lobe, which uncovered a new allosteric site. In addition, we demonstrate that DCLK1-IN-1 binds DCLK1 long isoforms with high affinity but does not prevent DCLK1 MAP function. Together, our work outlines the need for in-depth studies to rationally design of isoform-specific modulators and provides an invaluable structural platform to further the design of selective DCLK1 therapeutic agents.

Introduction

Doublecortin-like kinase 1 (DCLK1) is a large multi-domain bi-functional protein that belongs to both the protein kinase superfamily and the doublecortin (DCX) superfamily, within the microtubule associated protein (MAP) family. The tandem doublecortin domain (DCX1 and DCX2), located in the N-terminal region of DCLK1, drives its MAP function, while C-terminal region harbours an active serine/threonine kinase domain (Fig. 1a).

Beyond its established role in neurogenesis, DCLK1 has been identified as an intestinal and pancreatic stem cell maker[1-3] and growing evidence supports a role for DCLK1 in various malignancies. Many MAPs are known to play an important role in stabilization or destabilization of microtubules and changes in their expression levels are often associated with the development and progression of cancer[4,5]. Overexpression of DCLK1 has been reported in multiple cancers, including colon, pancreatic, renal cell carcinoma and rectal neuroendocrine tumours[6-10]. Aditionally, a relative high number of DCLK1 mutations have been identified in human gastric tumours[11,12].

The regulation of DCLK1 is highly complex and takes place at many levels, however it is poorly understood. Multiple isoforms of DCLK1 exist, generated by alternative promoter usage and alternative splicing[13-15]. These isoforms differ drastically in their domain composition and hence in their biological function. The most relevant functional differences between these isoforms lies in the presence or abscence of the N-terminal tandem doublecortin domains that contribute to DCLK1's MAP function. Two main human isoforms have been reported in the literature, DCLK1-long (DCLK1-L), which contains the tandem doublecortin domains at the N-terminus and a kinase domain at the C-terminus and DCLK1-short (DCLK1-S), which lacks the tandem doublecortin domains and contains only the C-terminal kinase domain[14,16,17]. For each of the DCLK1-L and -S isoforms, two other splicing variants exist (α and β), which differ in the length and sequence of the C-terminal regulatory tail that immediately follows the kinase domain. Unfortunately, the nomenclature used to describe the various DCLK1 isoforms has not been consistent over the years, as recently highlighted in the Swiss-Prot and NCBI databases[8,17], which has led to some discrepancy. Earlier studies in mice have demonstrated differential expresssion of spliced variants in embryonic and adult brains[16]. However, a lack of appropriate detection tools has rendered the study of the isoform specific expression patterns difficult. The detection of DCLK1 proteins in cells has been done using commercial antibodies that specifically target a C-terminal sequence that is not present in all isoforms[3,9,17]. Hence, the overall expression profile of DCLK1 isoforms in various tissues, the systematic evaluation of their biological function, and their relative contribution to tumorigenesis have been largely overlooked and remain to be investigated. Adding to this complexicity, recent studies have highlighted that DCLK1 undergoes epigenetic regulation. Hypermethylation of the DCLK1 5'(α) promoter in human colon adenocarcinomas (CRCs), resulted in the loss of DCLK1-L

isoform and the usage of an alternate β-promoter drove the expression of DCLK1-S isoform [17-19]. In addition, the cleavage of DCLK1 by the cysteine protease calpain has been reported in neurons, resulting in the release of the kinase domain from the tandem doublecortin domains, a mechanism proposed to drive the relocalisation of the kinase domain to the nucleus[20]. Corroborating these data, the nuclear transcription factor, Jun dimerization protein 2 (JDP2), was recently identified as a substrate for the zebrafish DCLK1 kinase domain[21]. Despite these studies, the calpain-dependent proteolytic regulation of DCLK1 is unclear and the functional relevance of DCLK1 kinase domain localisation to the nucleus remains to be established.

Developing targeted strategies for such a protein with isoform-specific functions and varying expression levels is therefore particularly challenging. The therapeutic effect of DCLK1 knockdown or silencing has been widely demonstrated in various cancer models[22-24], highlighting DCLK1 as an attractive target. The dual functions of DCLK1, as a MAP and as a kinase, may each contribute to tumorigenesis differently[25]. However, studies that demonstrate the direct impact of independently targeting DCLK1 kinase activity or its microtubule polymerization/stabilisation function and the potential effect on tumour growth are lacking. The lack of selective DCLK1 small molecule modulators that specifically target either DCLK1 kinase function or MAP function in isolation has precluded our understanding of the relative contribution of each function to oncogenicity. Most studies reported to date have commonly used as DCLK1 kinase inhibitors two compounds based on a benzopyrimido-diazipinone scaffold, the LRRK2 compound, LRRK2-IN-1 and the ERK5 compound, XMD8-92, as they both showed significant off target activity against DCLK1 kinase function[26,27]. However, their pan selectivity (targeting not only DCLK1) makes the published studies difficult to interpret with respect to DCLK1 kinase function. Recently, the Gray group has generated a bespoke highly selective DCLK1/DCLK2 inhibitor (DCLK1-IN-1) derived from this benzopyrimido-diazipinone series, as a way forward for dissecting the contribution of DCLK1 kinase activity on DCLK1 tumoregenesis activity[28].

Here, we present the crystal structures of DCLK1 kinase domain in complex with DCLK1-IN-1 and the two critical intermediates. Combined, our structural data rationalises the structure-activity relationship (SAR) behind DCLK1-IN-1 and provides the basis for DCLK1-IN-1 increased selectivity over ERK5 and LRRK2 kinases. Interestingly, binding of DCLK1-IN-1 induced a significant shift in the position of the N-lobe, which results in an opening of the ATP binding site and importantly uncovers a new allosteric site. Differences in the binding kinetics of DCLK1-IN-1 corroborate our structural data that demonstrate that DCLK1-IN-1 adopts an intermediate binding mode compared to the two precursors which bind in a conventional Type I binding mode. Combined, our data show that DCLK1 selectivity can be achieved with compounds capable of inducing such a conformational change. In addition, we rigorously highlight the complexity of DCLK1 regulation

and demonstrate that DCLK1-IN-1 binds to DCLK1 long isoform with high affinity but does not prevent DCLK1 MAP function. Such a result is in line with our data suggesting that kinase activity is required to prevent DCLK1 MAP function[25]. Taken together, our structural data presented here will undoubtedly provide a framework for the generation of highly selective and highly potent DCLK1 modulators and chemical probes (inhibitors or targeted protein degraders), for future therapeutic intervention.

Results

Crystal structure of DCLK1 in complex with benzopyrimido-diazipinone scaffold molecules

The potent activity of multiple compounds based on a 5, 11-dihydro-6H-benzo[e]pyrimido[5,4-b][1,4]diazepin-6-one scaffold (Fig. 1a) towards the kinase family is well established and several studies have demonstrated the excellent potential of this scaffold as a starting point for kinase drug discovery[29-32]. The benzopyrimido-diazipinone scaffold family of compounds, that include the LRKK2 kinase inhibitor, LRRK2-IN[33], and the ERK5 inhibitors XMD8-92 and XMD8-85[34] warranted further development, displaying significant off target activities against PLK1 and PLK3, DCLK1 and DCLK2, as well as the bromodomains of BRD4[34-36]. Recently, DCLK1-IN-1 was reported as a selective DCLK1/DCLK2 inhibitor derived from modifications of this 5,11-dihydro-6H-benzo[e]pyrimido[5,4-b][1,4]diazepin-6-one scaffold[28,37]. Optimisation of DCLK1-IN-1 was achieved through modifications at R1 and R4 positions, which enhanced DCLK1 selectivity by reducing binding to ERK5 and BRD4[28]; modifications at R2 and R3 did not improve selectivity (Fig. 1a).

We had previously demonstrated the ability of LRRK2-IN-1 and XMD8-92 to bind to purified recombinant DCLK1 kinase domain (DCLK1-KD) using a thermal stability assay[25]. However, despite attempts to crystallise these inhibitors in complex with DCLK1 kinase domain (DCLK1-KD), we never obtained diffraction quality crystals, likely due to the weak affinity of these inhibitors. We therefore took advantage of the availability of more potent DCLK1 benzopyrimido-diazipinone scaffold inhibitors such as XMD8-85 to utilise for crystallography, so as to provide a structural framework to further guide the development of DCLK1 selective tools.

We first confirmed the ability of DCLK1-IN-1's precursor, XMD8-85, and subsequently DCLK1-IN-1, to bind to DCLK1-KD (residues 372-649) by carrying out thermal stability assays (Fig. 1b, Supplementary Fig. 1). We used DCLK1-NEG, a structurally related negative control compound, which was predicted to have significantly reduced affinity for DCLK1, owing to incorporation of an additional methyl substituent at R3 (Fig. 1a) that would cause steric clash with residues located at the start of the activation loop and near the floor of the ATP binding site[25]. By performing a compound titration between 2.5 μM and 40 μM, we demonstrated an increased shift in the melting temperature

of DCLK1-KD as the concentration of the compounds increased, confirming that both XMD8-85 and DCLK1-IN-1 bind DCLK1-KD. As expected, the DCLK1-NEG compound showed severely reduced binding to DCLK1-KD (Fig. 1b and Supplementary Fig. 1).

Crystal structure of DCLK1-KD:XMD8-85*:* To understand the structural basis by which XMD8-85 increased inhibition of DCLK1 as compared to XMD-8-92 and to elucidate its retained pan-activity against ERK5 and LRRK2, we solved the structure of DCLK1-KD (residues 372-649) in complex with XMD8-85 to 2.5 Å (Fig. 2a, Supplementary Table 1, Supplementary Fig. 2). The DCLK1-KD:XMD8-85 complex crystallised with two molecules in the asymmetric unit with a head to tail packing similar to DCLK1-KD:AMPPNP (5JZJ) and DCLK1-KD:NVP-TAE684 (5JZN) crystal structures (Fig. 2a and b) that we solved previously[25]. However, the "face-to-face" arrangement previously seen in these structures, promoted by the packing of an extended αC helix from one molecule against the activation loop of the second molecule, is not observed in this new structure. In the DCLK1-KD:AMPPNP and DCLK1-KD:NVP-TAE684 structures, this unusual activation loop dimerization mode was found to be stabilised by the coordination of a sulfate molecule between Arg510 from the catalytic loop of one molecule and Thr546 from the activation loop of the other (sulfate occupying the position where a phosphate would be if the protein was phosphorylated on the activation loop) (Fig. 2b). In DCLK1-KD:XMD8-85 structure, the sulfate coordination is no longer maintained. Despite this, the activation loop is entirely visible and adopts an active conformation state (Fig. 2a). This active conformation state is further confirmed by the presence of the canonical salt-bridge interaction between the conserved αC helix glutamate (Glu436) and the invariant β3 strand lysine (Lys419) (Fig. 2c) . However, the extended αC helix conformation previously reported is not seen (Fig. 2a and b**)** [25]. Instead, an additional turn in the αC helix is visible (Fig. 2c). Residues 424-430, that were previously involved in crystal packing in the NVP-TAE684 structure, could not be modelled, highlighting the inherent flexible property of the αC helix in DCLK1 to accommodate the binding of XMD8-85. Additionally, XMD8-85 induces a conformational change in the glycine loop and residues 399-400 located at the tip of the glycine loop also could not be modelled (Fig. 2c). While the position of ring C of XMD8-85 aligns with ring B of NVP-TAE684, both ring A and B of XMD8-85 sit deeper into the backpocket within the ATP binding site (Fig. 2d). XMD8-85 is further stabilised by van der Waals (vdw) interactions between ring A and Gly532 (that preceeds the DFG motif) and between ring B and Val449 (that is located between αC helix and β5 strand) (Fig. 2c). Mutation of Gly532 to valine considerably reduces XMD8-85 binding affinity for DCLK1-KD (Supplementary Fig. 3), likely by causing a steric clash.

The interaction of XMD8-85 with DCLK1-KD results in two hydrogen bonds interactions within the ATP binding site **(**Fig. 2e**)**. These all occur through interaction of XMD8-85 within the hinge region,

involving a donor/acceptor hydrogen bond pair with the backbone of Val468. The amine group (N2) in the linker between rings D and C of XMD8-85 acts a hydrogen bond donor for the backbone carbonyl oxygen of Val468, and the amine group (N5) in ring C of XMD8-85 acts as an acceptor for the backbone amide -NH of Val468. Additionally, the hinge region residues Gly471 and Lys469 further stabilise ring D conformation through main chain interactions. Residue Leu518 located on β7 at the floor of the ATP binding pocket also stabilises rings A, B and C through hydrophobic/vdw interactions. Notably, the amide carbonyl oxygen of diazepine ring B participates in a network of water-mediated hydrogen bond interaction with the invariant Lys419 and αC Glu436 that play a critical role in nucleotide binding **(**Fig. 2f and 2g). The amide N-methyl subsitutent at position R4 on diazepine ring B confers significant affinity for DCLK1. This R4 N-methyl group is able to form favourable vdw interactions with the gatekeeper residue Met465 (on β5) located at the back of the ATP binding site as well as Ala417, Val449 and Glu466 **(**Fig. 2e**)**. Removal of the N-methyl group was demonstrated to result in a loss of affinity towards DCLK1, ERK5 or BRD4, but led to a modest reduction in affinity for LRRK2[28]. As for DCLK1, LRRK2 has a gatekeeper methionine residue, suggesting that for LRRK2 this residue is not a significant contributor to the observed affinity[38]. Interestingly, the salt bridge interaction between residue Glu415 (β3 strand) and Lys469 from the hinge region is maintained, acting as anchor point to maintain the structural integrity of this interface (Fig. 2e). The structure also revealed other features of XMD8-85 that likely account for its improved DCLK1 affinity relative to XMD9-92. In particular, the ortho methoxy substituent in ring D in XMD8-85 is likely better accommodated in DCLK1 than the bulkier ortho ethoxy substituent of XMD8-92; secondly, protonation of the para N-methylpiperazine of XMD8-92 at physiological pH would enable an additional favourable electrostatic interaction with Asp475 of DCLK1, which isn't possible for the ortho 4-hydroxypiperidine subsituent of XMD8-92[28]. However, the DCLK1-KD:XMD8-85 crystal structure also revealed aspects of sub-optimal shape complementarity of XMD8-85 for the DCLK1 ATP binding site and additional cavities near the back pocket that might be exploited to improve selectivity towards DCLK1 (Fig. 2g and 2h). Overall, our DCLK1-KD:XMD8-85 crystal structure clearly indicated that the N-methyl group in the R4 position is orientated towards the gatekeeper residue Met 465, such that modifications in this position might be used to improve specific selectivity for DCLK1, in particular relative to other kinases with a differing gatekeeper residue.

R4 modification provides increased selectivity towards DCLK1: Based on our structural information, Ferguson et al., designed two compounds FMF-03-055-1 and FMF-03-146-1 (DCLK1-IN-1) by respectively introducing ethyl and triflouroethyl substituents at the R4 position (Fig. 1a). We reasoned that modifications at the R4 position might increase selectivity towards DCLK1 by targeting the deep hydrophobic back pocket surrounded by residues Leu440, Val449, Met465 and the backbone of the

DFG loop (Fig. 2h). In addition, considering the conformational variability of the αC helix observed in the DCLK1-KD:XMD-8-85 structure as compared to ether the DCLK1-KD:AMP-PN or DCLK1-KD:NVP-TAE684 structures (Fig. 2a and 2b), it was conceivable that these modifications might induce DCLK1 kinase domain to adopt an inactive conformation.

As illustrated by compound FMF-03-055-1, introduction of a N-ethyl substitution at position R4 was well tolerated by DCLK1 and in fact resulted in 5-fold enhanced potency for DCLK1 as compared to XMD8-85[28,37]. This modification also reduced off-target binding to both ERK5 and BRD4, but only to a limited extent for LRRK2[28]. LRRK2 (humanized ROCCO4), has identical residues to DCLK1 within the ATP binding pocket, including the gatekeeper methionine, which could explain this observed retention of potency with this modification (PDB:4YZM[38]).

To better understand how the ethyl substitution at position R4 provided increased potency towards DCLK1 and increased selectivity over ERK5, we solved the crystal structure of DCLK1-Cter:FMF-03-055-1 (residues 372-686) to 3.1Å resolution (Fig. 3a, Supplementary Table 1). The ATP binding site shows a clear unbiased electron density for FMF-03-055-1 (Supplementary Fig. 2). The presence of the ethyl group at the R4 position in FMF-03-055-1 has not changed the position of the benzopyrimido-diazipinone scaffold within the ATP binding pocket. The backbone H-bond interactions mediated by Val468 located in the hinge region are still conserved in DCLK1-Cter:FMF-03-055-1 (Fig. 3b). Our crystal structure reveals that the ethyl group in FMF-03-055-1 indeed mediates additional contacts with Lys419, Ala417, Val404 and the gatekeeper residue Met465 as compared the methyl in XMD8-85 (Fig. 3b). In addition to enhancing binding to DCLK1, the ethyl substitution also significantly decreased off-target binding to ERK5. This could be attributed to the presence in ERK5 of a leucine instead of a methionine as the gate keeper residue (Leu137). While a leucine residue is shorter, it has more constrained side chain conformations compared to a methionine. Analysis of ERK5:XMD8-92 (PDB 5BYY) structure indeed suggests that ethyl group substitution at position R4 would result in a clash with Leu137 in its current rotamer conformation (Fig. 3c). Our structural data therefore provides the rationale for the increased affinity of FMF-03-055-1 towards DCLK1 and its loss of affinity towards ERK5. Conversely, the higher affinity of XMD8-92 towards ERK5 compared to DCLK1 can be attributed by the collapse of the N- towards the C-lobe resulting in a tight binding of this compound (XMD8-92 IC_{50} for ERK5 is 98nM (Fig. 3d)[34].

DCLK1-IN-1 selectively binds DCLK1-KD: While the R4 ethyl group in FMF-03-055-1 enhanced affinity towards DCLK1 and decreased off-target affinity for ERK5, FMF-03-055-1 still showed appreciable binding to LRRK2 and BRD4[28]. To further probe the R4 position, an electronegative trifluorethyl group was introduced instead of hydrophobic ethyl, which led to the compound known

as DCLK1-IN-1[37]. Interestingly, DCLK1-IN-1 showed modest reduction in affinity for DCLK1 compared to FMF-03-055-1 but simultaneously a significant improvement in selectivity against ERK5, LRRK2 and BRD4[37]. To better understand the effect of this change, we crystallised DCLK1-KD in complex with DCLK1-IN-1 to 3.1Å resolution (Fig. 4a and 4b). The DCLK1-KD:DCLK1-IN-1 complex crystallised in a similar head to tail conformation as seen for the DCLK1-KD:XMD8-85 and DCLK1-Cter:FMF-03-055-1 structures (Fig. 2a, 3a and 4a). The ATP binding site shows a clear unbiased electron density for DCLK1-IN-1 (Supplementary Fig. 2). Overall, the substitution of the methyl or ethyl group at position R4 with the trifluoroethyl group does not affect the conformation of the Met465 side chain nor the conformation of the αC helix or the A-loop (Fig. 4c). However, a striking feature of the DCLK1-KD:DCLK1-IN-1 structure, compared to DCLK1-KD:XMD8-85 and DCLK1-KD:FMF-03-055-1, is a significant opening of the ATP binding site, whereby both the glycine loop and the β3 strand undergo an upward shift of 5Å to accommodate the bulkier trifluoroethyl group (Fig. 4c and 4d). As a likely consequence of this effect due to binding of DCLK1-IN-1, no electron density was observed for residues 397-401 from the glycine loop, highlighting its high flexibility. However, the specific orientation adopted by the trifluoroethyl group allows additional contacts with residues Ala417, Val404, Ala417 and Met465 (Fig. 4b). Significantly, the presence of the trifluoroethyl group, which also causes a significant shift in the position of the β strands that make the N-term lobe (Fig. 4c), disrupts the salt-bridge interaction between the invariant lysine (Lys419) of β3 strand with the conserved glutamate (Glu436) of the αC helix **(**Fig. 4c**)**. Interestingly, this opening creates a new shallow pocket, which is in our structure occupied by extra electron density that could be attributed to a fragment of polyethylene glycol (PEG), a component of the crystallisation condition (Fig. 4c). Significantly, this shallow pocket, surrounded by the αC helix, the activation loop DFG motif and the β3 strand lysine (Lys419), represents a novel DCLK1 allosteric site, unseen in other DCLK1 structures solved to date (Fig. 4c and 4d). A similar allosteric site has been reported in ERK5 when bound to an allosteric inhibitor (Supplementary Fig. 4)[34].

Together, our structural data demonstrates that in contrast to XMD8-85 and FMF-03-055-1, which adopt a conventional type I binding mode (Fig. 2c and 3b), DCLK1-IN-1 adopts a type 1.5 binding mode with DCLK1 by inducing a large conformational change in the N-lobe and a creating a new allosteric site (Fig. 4c and 4d). These changes can account for the dramatically increased DCLK1-IN-1 selectivity for DCLK1 against ERK5, LRRK2 and BRD4[37].

DCLK1 isoforms: considerations to be taken when designing DCLK1 selective tools to study DCLK1 in the context of cancer.

Several studies have shown the beneficial effect of DCLK1 knockdown on tumor growth[10,24,39-41] Considering the dual biological function of DCLK1 and the presence of multiple isoforms (Fig. 5a

and Table 1), understanding the role of DCLK1 in cancer development and progression is likely to require mechanistic studies that pinpoint and dissect the expression pattern and the contribution of each DCLK1 isoform. Unfortunately, several of the studies published to date do not provide such comprehensive expression data. To begin to dissect the underlying mechanisms that link DCLK1 to oncogenesis and evaluate the use of DCLK1-selective inhibitors, we summarise those studies which investigate the specific role of distinct DCLK1 isoforms. In colorectal cancer (CRC), DCLK1-S isoforms, which lacks the microtubule binding domain, are reportedly overexpressed in several codon 12 KRAS mutant cells including G12D[42]. Likewise, human colon adenocarcinomas (hCRCs), overexpress DCLK1-S from an alternate (β)-promoter of DCLK1, due to the epigenetic silencing of the 5'(α)-promoter, which results in the specific loss of the DCLK1-L isoform. In addition, high expression of DCLK1-S is also associated with a significantly worse overall survival rates[17]. Therefore, DCLK1 kinase inhibition, using an inhibitor such as DCLK1-IN-1, may be suitable to further study the role of DCLK1-S in these cancer models.

In non-small cell lung cancer (NSCLC), DCLK1-S isoform is predominantly over-expressed in cell lines H460 and A549, whereas DCLK1-L isoform is predominantly expressed in H1299 cells[39]. However, the specific functions of each of the DCLK1 isoforms and their regulation of NSCLC remains unclear and requires futher study. Similarly, in renal clear cell carcinoma (RCC), the most common type of kidney cancer, both DCLK1-S and DCLK1-L isoforms are over-expressed (Table 1). Tumors expressing DCLK1-L isoform are enriched in cancer stem cell markers, however, tumors expressing DCLK1-S do not show such enrichment. While DCLK1-L has been shown to drive molecular and functional stemness[43], the role of DCLK1-S in RCC remains unclear and will require further clarification.

In addition to the differential expression profiles observed for each isoform in various cancers, the expression levels of a particular isoform can vary between the early and late stages of a particular cancer type. For example, the levels of DCLK1-L in the serum of patients with pancreatic ductal adenocarcinoma (PDAC) significantly varies between early and advanced stages[44]. Interestingly, DCLK1-IN-1 seems ineffective on PDAC cells lines, PATU-8988T and PATU-8902, and was only effective on organoid samples isolated from an early stage of the disease but not from the advanced stage, despite all expressing DCLK1-S isoforms[37]. Unfortunately, this study did not specifically look at differences in levels of DCLK1-L, nor have the differences in DCLK1-S expression levels between the early and late stages of pancreatic cancer been reported. Thus, it is possible that either a lower DCLK1-S expression, or an altered DCLK1-L expression, in the late stage of pancreatic cancer could explain the lack of DCLK1-IN-1 activity. Together, these studies highlight an urgent need for a greater understanding of DCLK1 isoforms expression patterns, their differential expression levels

during the various stages of cancer, as well as their epigenetic regulation in order to design the best therapeutical strategy.

DCLK1-IN-1 binds DCLK1-L isoforms

***The presence of the DCX domains does not prevent DCLK1-IN-1 binding to the kinase domain*:** To begin to unravel if a selective DCLK1 kinase inhibitor can target DCLK1 long isoforms, we first sought to determine if the presence of the N-terminal doublecortin domains and additional N- and C-regulatory elements impacted DCLK1-IN-1 binding to the DCLK1 kinase domain by thermal shift assay (TSA). We generated two DCLK1-L (Uniprot O15075-2) constructs: DCLK1-FL1Δ (residues 50-686) and DCLK1-FL2Δ (residues 1-700) (Fig. 5a). Both constructs were generated as WT (phosphorylated), and as a catalytically dead D511N mutant. However, the level of protein recovered from DCLK1-FL2Δ D511N was too little to allow further studies. We hence tested DCLK1-FL1Δ for its ability to bind DCLK1-IN-1 using thermal shift assay[45]. Similar to DCLK1-KD, DCLK1-FL1Δ WT and the equivalent D511N mutant showed a marked upward shift in melting temperature with increasing concentration of DCLK1-IN-1, as compared to the control compound DCLK1-NEG, suggesting binding (Fig. 5b and Supplementary Fig. 5).

***Kinetic mechanism of inhibitor binding explains lower potency of DCLK1-IN-1**:* While the trifluoroethyl group substitution led to a dramatically increased selectivity of DCLK1-IN-1 for DCLK1, it resulted in a 5-fold reduction in DCLK1 potency [37]. Having established that DCLK1-IN-1 binds to DCLK1-L isoforms by TSA, we next wanted directly quantify the affinity of this interaction. We therefore took advantage of the availability of our DCLK1 long construct (DCLK1-FL1Δ - residues 50-686) to carry out a comparative analysis of binding kinetics of each inhibitor using Surface Plasmon Resonance (SPR), as it would allow simultaneous assessment of both affinity and kinetics. Both the non-phosphorylated (DCLK1-FL1Δ D511N) and phosphorylated wild-type (DCLK1-FL1Δ WT) proteins were immobilised to the sensor chip. We focused our analysis on DCLK1-FL1Δ D511N but similar data were obtained for the WT protein (Table S2, Figure 5c, Supplementary Figures S6, S7, S8). The measured binding affinity of DCLK1-IN-1 for DCLK1-FL1Δ D511N (K_D = 53 nM) (Figure 5c Supplementary Table S2) broadly parallels the affinity of DCLK1-IN-1 for DCLK1-KD previously determined by ITC (reported with a K_D of 55 nM and 109 nM in[37]). In combination with our TSA data (Figure 5b), this suggests that DCLK1-IN-1 can likely bind with relatively high affinity to either DCLK1-S or DCLK1-L isoforms, in either phosphorylated or non-phosphorylated states. Whilst direct affinity measurements for FMF-04-055-01 and XMD8-85 have not been previously reported, our SPR-determined direct affinity values for FMF-04-055-01

and XMD8-85 binding to DCLK1-FL1Δ D511N showed similar trends to reported IC_{50} values for inhibition of DCLK1-KD in a competitive displacement assay[37], although in our hands XMD8-85 appeared to bind DCLK1 with slightly stronger affinity than that suggested by the reported inhibitory IC_{50}. As expected, DCLK1-NEG showed only weak binding to DCLK1 (K_D > 10 μM). Consistent with earlier observations, we found that by SPR the affinity of DCLK1-IN-1 for DCLK1-FL1Δ D511N (K_D = 53 nM) was relatively weaker (approximately 4-5 fold) than either FMF-04-055-01 (K_D = 13 nM) or XMD8-85 (K_D = 8 nM). This difference is a function of both the on- and off-rates of binding to DCLK1. DCLK1-IN-1 exhibits both a slightly slower on-rate (~2-fold) and a slightly faster off-rate (~2-fold), relative to either FMF-04-055-01 or XMD8-85, for which the kinetics are similar. This difference in kinetics is consistent with our structural data, which suggests that a greater conformational adjustment to the N-lobe of DCLK1 (including opening of the ATP binding site) is required to accomodate the binding of DCLK1-IN-1, compared to either FMF-04-055-01 or XMD8-85 (Fig. 4d).

DCLK1-IN-1 does not inhibit DCLK1 MAP function: Having established that DCLK1-IN-1 binds to DCLK1-L isoform with a similar affinity to the DCLK1 kinase domain, we next wanted to show if DCLK1-IN-1 binding had an impact on DCLK1 MAP function. We and others have previously shown that purified DCLK1 promotes tubulin polymerisation *in vitro*[25,46]. We additinonally showed that DCLK1 kinase domain activity regulates its tubulin polymerization activity[25]. Using a fluorescent based polymerisation assay, we previously demonstrated that phosphorylated DCLK1 full-length no longer polymerises tubulin and DCLK1's tubulin polymerisation activity could be restored upon phosphatase treatment or when using a catalytically dead mutant protein, DCLK1-D511N. We again took advantage of this mutant to determine if binding of DCLK1-IN-1 to the kinase domain had an impact on DCLK1 tubulin polymerisation activity using microtubule polymerisation and pelleting assays, followed by analysis by SDS-PAGE of the supernatant and pellet fractions. We first performed a phos-tag gel analysis to confirm the difference in phosphorylation between phosphorylated DCLK1-FL1Δ WT and DCLK1-FL1Δ D511N (Supplementary Fig. 7). We next tested tubulin polymerisaton in the presence of phosphorylated DCLK1-FL1Δ WT and the corresponding catalytically dead mutant D511N. As expected, DCLK1-FL1Δ WT does not polymerise tubulin (Fig. 5d, lanes 1-2) while the catalytically dead mutant D511N does (Fig. 5d, lanes 3-4), as seen by the increased presence of tubulin (and DCLK1 D511N) in the pelleted fraction. This is consistent with our previous observation using tubulin polymerisaton assays based on fluorescence-based dye (Cytoskeleton Inc)[25]. We next tested tubulin polymerisation in the presence of 20 μM and 40 μM DCLK1-IN-1, concentrations which showed binding to DCLK1 based on our TSA data (Fig.

5b). The presence of DCLK1-IN-1 at 20 μM (Fig. 5d, lanes 5 and 7) or 40 μM (Fig. 5d, lanes 8-9) does not affect tubulin polymerisation capability of DCLK1-FL1Δ D511N compared to the control condition without the compound (Fig. 5d, lanes 3-4). We confirmed that the addition of 40 μM DCLK1-IN-1 does not cause DCLK1-FL1Δ D511N to aggregate and pellet upon centrifugation (Fig.5d, lanes 12-13). We also confirmed that DCLK1-IN-1 alone does not promote tubulin polymerisaton in the absence of DCLK1-FL1Δ D511N, (Fig. 5d, lanes 10 -11). As negative control, we tested tubulin polymerisation in the presence of nocodazole, a well-characterised microtubule destabliser. As expected, the presence of 40 μM nocodazole inhibits tubulin polymerisation (Fig. 5d, lanes 14-15), while the presence of 40 μM of DCLK1-NEG compound has no impact on tubulin polymerisation (Fig. 5d, lanes 17-20). Nocodazole has been suggested to target both kinases and microtubules[47]. We therefore confirmed whether nocodazole was capable of binding DCLK1 using thermal stability assays (Supplementary Fig. 7). Nocodazole does not bind DCLK1 at 40uM and hence the inhibition of tubulin polymerisation observed in the presence of nocodazole can be solely attributed to tubulin destabilisation. To further confirm the lack of DCLK1-IN-1 activity on DCLK1 MAP function, we carried out a fluorescence-based Tubulin Polymerisation Assay (Cytoskeleton)[25]. As expected, the catalytically dead mutant DCLK1-FL1Δ D511N is capable of inducing tubulin polymerization in vitro (Supplementary Fig. 7). Adding DCLK1-IN-1 at 20 μM or 40 μM has no impact on tubulin polymerisation capability of DCLK1-FL1Δ D511N (Fig. 5e) and as expected Nocodozale (80 μM) completely inhibits tubulin polymerisation. We confirmed that DCLK1-IN-1 or DMSO in this sample does not promote tubulin polymerisation in the absence of DCLK1-FL1Δ D511N (Fig. 5e). Collectively, these results suggests that DCLK1-IN-1 does not have an effect on the DCLK1 MAP function. Hence, this highlights the need for future studies utilising DCLK1-IN-1 in the context of cancer to clearly define the role of the kinase function in driving the cancer under investigation.

Discussion

DCLK1 is widely recognised as a potential therapeutic target of interest in cancer. DCLK1 deregulation has been reported in various cancers, including gastric, pancreatic, breast, colorectal and kidney. As outlined, DCLK1 harbours two distinct functions, a kinase and a MAP function and DCLK1 isoforms encode either only one of these two functions or both. There is clearly an emerging appreciation that distinct DCLK1 isoform signatures may exist in cancer development and progression, calling for in-depth studies to rationally design isoform-specific modulators and develop effective therapeutic strategies. Recently, the Gray group published DCLK1-IN-1, a selective DCLK1

kinase inhibitor elaborated from a benzopyrimido-diazipinone scaffold, a much needed tool to dissect the contribution of DCLK1 kinase activity to oncogenesis.

Here, we provide a structural basis for the design of DCLK1-IN-1 and demonstrate how selectivity of DCLK1-IN-1 for DCLK1 can be achieved over ERK5 and LRRK2. The structures of DCLK1-KD in complex with the three benzopyrimido-diazipinone scaffold analogues revealed that the tricyclic ring system induces a significant conformational change in the glycine loop and in the relative position of the N-lobe β-strands to the C-lobe, without impacting the activation loop, which is well resolved and in an active conformation. As per NVP-TAE864, both XMD8-85 and FMF-03-055-1 inhibitors bind in a conventional type I binding mode and in both cases the glycine loop collapses allowing extensive interactions with ring B and ring D contributing to the compound's affinity towards DCLK1. However, rings A and B of XMD8-85 sit slightly deeper into DCLK1 ATP binding site compared to NVP-TAE864, suggesting a greater access to the back pocket. The key positioning of the methyl group at position R4 towards the gate keeper residue and the difference in the nature of the gate keeper residue between DCLK1 and ERK5 have highlighted how selectivity for DCLK1 over ERK5 could be achieved. The introduction of an ethyl group at position R4 in FMF-03-055-1 further capitalised on the altered properties of the back pocket between DCLK1 and ERK5 and led to a dramaticly increased selectivity of FMF-03-055-1 for DCLK1 over ERK5.

Both XMD8-85 and FMF-03-055-1 were shown to be further stabilised by van der Waals interactions between ring A and Gly532 that precedes the DFG motif, interactions that are likely contributing to the stabilisation of the activation loop in an active conformation. Importantly for both of those structures, the structural integrity of the ATP binding site was maintained via the canonical salt bridge interaction between β3 strand lysine (Lys419) and the αC helix glutamate (Glu436).

In contrast, the crystal structure of DCLK1-KD:DCLK1-IN-1 revealed a different binding mode. We showed that the substitution of the hydrophobic ethyl with an electronegative trifluorethyl group causes a significant opening of the ATP binding site through disruption of the canonical salt-bridge interaction between the invariant β3 strand lysine (Lys419) and the αC helix glutamate (Glu436), leading to an anticlockwise rotation of the N-lobe from the hinge gate keeper residue. Importantly, the orientation of the αC helix and the conformation of the activation loop both remain unchanged. These critical features, together with the drastic opening of the ATP binding site, contribute to the formation of a new allosteric site in a shallow pocket surrounded by the αC helix, the DFG motif and the invariant β3 strand lysine. This unusal binding mode classifies DCLK1-IN-1 as a type 1.5 inhibitor, with DCLK1 kinase domain adopting an intermediate conformation. Conservation of the αC orientation upon binding of an allosteric compound has been reported for ERK5. However, in ERK5, allosteric inhibitors were shown to bind into a pre-existing allosteric site near the ATP binding site, with the binding inducing the displacement of the glycine loop into the ATP-binding site. In

DCLK1, the binding of DCLK1-IN-1 to the ATP binding site causes a large conformational change in glycine loop, which in turns create an allosteric pocket adjacent to the ATP binding site.

The discovery of this induced allosteric site raises an interesting prospect in developing DCLK1 selective inhibitors that can fully capitalise on this site. Currently, DCLK1-IN-1 showed a clear gain in selectivity towards DCLK1 over ERK5 and the other off-target kinases, albeit a 5-fold reduction in affinity compared to FMF-03-055-1. Our SPR data clearly indicate that the reduction in affinity reflects subtly altered binding kinetics, results that are consistent with opening of the binding cleft. Together, this data strongly suggests a significant plasticity of the DCLK1 kinase domain which can be pushed to adopt an intermediate conformation. An inhibitor with type 1.5 binding mode is therefore likely to be more selective than the typical type I inhibitors, such as XMD8-85 and FMF-03-055-1. In addition, the significant increase in selectivity over ERK5 can be mainly attributed to the difference in gatekeeper residue, which in addition to guarding the accessibility of the back pocket may dictate the differential flexibility of the N-lobe/glycine loop at the hinge point, a feature that is kinase dependent[48].

The selectivity of DCLK1-IN-1 now allows the interrogation of the biological kinase functions of DCLK1 isoforms that contain the kinase domain. So far, DCLK1-IN-1 has been shown to be efficient in only a subset of patient derived organoid samples that expressed DCLK1-S[37]. The use of DCLK1-IN-1 in colorectal cancer cell line model has also recently allowed a connection to be established between DCLK1 and RNA processing pathways, although it is not clear in this study which isoform was overexpressed[49]. Regardless, DCLK1-IN-1 represents an invaluable tool to specifically dissect the biological kinase function of the DCLK1-short isoforms and their contribution to tumorigenesis.

However, the overall value of targeting the kinase activity with an ATP competitive inhibitor in a full-length context remain questionable. DCLK1 promotes tubulin polymerisation through its DCX domains[46]. We previously demonstrated that DCLK1 kinase activity plays a critical role in regulating microtubule dynamics through autophosphorylation events. Phosphorylated DCLK1 no longer polymerise tubulin (this study and[25]). This is in agreement with a previous report indicating that deletion of the kinase domain enhances microtubule-binding activity[50].

Our data clearly shows that DCLK1-IN-1 binds DCLK1-L, whether phosphorylated or not (TSA, SPR data). The binding of DCLK1-IN-1 to non phosphorylated DCLK1-L does not disrupt the ability of the protein to polymerise tubulin (assays). The microtubule binding affinity of several MAPs (i.e. Doublecortin, Tau, MAP2) and their subcellular localisation are tightly regulated by phosphorylation events[51,52] and in most cases, phosphorylation negatively affect microtubule binding[53]. While the binding of DCLK1-IN-1 to the kinase domain does not seem to impact DCLK1 tubulin polymerisation activity, it is likely to prevent DCLK1 kinase domain from modulating DCLK1

microtubule binding through phosphorylation. Interestingly, our previous structural characterisation of presumed pathological mutations found in DCLK1-L in the context of gastric cancers, indicated that mutations occurring within the kinase domain would lead to a kinase disfunction. Together these data point towards a role for the kinase domain in regulating DCLK1 microtubule binding affinity and consequently its tubulin polymerisation activity. From these observations, it is clear that DCLK1-isoform specific targeting strategies will be required to account for their distinct biological functions. Evidence is accumulating on the benefit in reducing DCLK1 expression levels to reduce tumorigenesis. Our structures will provide the basis to develop a chemically induced degradation strategy, such as proteolysis-targeting chimeras (PROTAC)[54,55], in which a DCLK1 selective kinase-binding moiety might provide the necessary handle to recruit DCLK1 for degradation, thereby also dismantling DCLK1 MAP function.

In conclusion, the DCLK1-KD crystal structures presented here in the presence of benzopyrimido-diazipinone scaffolds have revealed a remarkable plasticity of the DCLK1 ATP binding pocket and additionally identified a novel allosteric site not seen previously. The existence of distinct DCLK1 isoform signatures in cancer progression and development calls for in-depth studies to rationally design isoform-specific modulators. Our study now establishes a structural framework as a platform to guide the design and development of novel isoform-specific modulators as therapeutic agents.

Material and Methods

DNA Constructs

Human DCLK1 (Uniprot O15075-2) constructs for protein expression were cloned into a modified pCOLD vector encoding an N-terminal tobacco etch virus protease cleavage site and an 8XHis tag (Takara). The constructs for the catalytically dead mutant was designed using primers containing the mutation, and PCR products were cloned in pCOLD vector. All constructs were verified using Sanger Sequencing (Micromon).

Recombinant protein expression and purification

Truncated DCLK1 constructs, DCLK1-KD (residues 372-649), DCLK1-Cter (residues 372-686) or DCLK1 FL1Δ (residues 50-686) and DCLK1 FL2Δ (residues 1-700), were expressed overnight at 16°C for 16 to 20 hours in *E. coli* C41(DE3) as previously described[25]. For crystallization, proteins were expressed in the presence of lambda phosphatase for homogeneity[25]. DCLK1 proteins were purified by Ni^{2+} affinity chromatography and size exclusion chromatography followed by anion exchange chromatography. Isolated proteins were concentrated to 5mg/ml and flash frozen in 20 mM Tris pH 7.5, 200 mM NaCl, 5% v/v glycerol, 0.5 mM TCEP.

Thermal Shift Stability Assay

Thermal shift stability assays were performed as described previously[45]. DCLK1 proteins were diluted in 150 mM NaCl, 20 mM Tris pH 8.0, 1 mM DTT to 2.5 mM final concentration and assayed with the appropriate concentration of inhibitor in a total reaction volume of 25 µL. SYPRO Orange (Molecular Probes) was used as a fluorescence probe and detected at 530 nm. The data shown are representative of two independent experiments.

Crystallization, Structure Determination, and Refinement

Crystallographic conditions were modified from Patel *et. al*[25]. For all the DCLK1-inhibitor complex crystals, purified DCLK1-KD or DCLK1-KD-Cter (5 mg/ml) was pre-incubated with 0.25 mM of compound prior to crystallisation trials. DCLK1-KD was co-crystallized with XMD-8-85 and DCLK1-IN-1 at room temperature in 2-4% PEG 400, 1.7- 2.3 M ammonium sulphate Hepes pH 6.5-7.25 and 0.5mM TCEP. DCLK1-KD-Cter (5 mg/ml) was co-crystallised with FMF-03-055-1 at 20°C in 0.2 M MgCl2, 30% PEG 4000, 0.1 M Tris pH 7.75 and 0.2 M $MgCl_2$, 31% PEG 4000, 0.1 M Tris pH 7.02, respectively, using the Bio21 C3 Collaborative Crystallization Centre. Crystals were flash frozen prior to data collection using glycerol as the cryoprotectant. The data were collected at 100K on the MX2 beamline at the Australian Synchrotron, Melbourne. The data were processed using iMosflm and XDS[56,57], respectively and scaled using AIMLESS from the CCP4 Suite. The DCLK1 inhibitor structures were solved by the molecular replacement method using PHASER in CCP4, with DCLK1-KD structure (PDB 5JZJ) as a model. The structures were refined using Phenix.refine.[58] Model building was carried out using COOT[59]. The ligand was modelled using the Grade Web Server . The overall structure were validated using MOLPROBITY. All molecular graphics representations were created using PyMOL (The PyMOL Molecular Graphics System, Version v1.8.0.3, Schrödinger LLC).

Surface Plasmon Resonance

Immobilisation. Proteins were immobilised at 25°C using standard amine coupling to a CM5 chip (GE Healthcare) in immobilisation buffer consisting of 10 mM HEPES pH 7.4, 150 mM NaCl, 1 mM TCEP, 0.005% Tween P20, 1% (v/v) DMSO. To the active flow cells were coupled either DCLK1 FL1Δ D511N or WT (each 2 uM in 10 mM sodium acetate buffer pH 4.0, supplemented 10 µM FMF-03-149-01 and 1% (v/v) DMSO final [28] to a final density of approximately 7000 RU, followed by surface deactivation with 1 M ethanolamine. A blank immobilisation was performed on the reference flow cell.

Binding studies. Binding experiments were performed at 18°C in running buffer consisting of 20 mM HEPES, 150 mM NaCl, pH 7.4, 1 mM tris(2-carboxyethyl)phosphine (TCEP), 0.005% (v/v) Tween-P20, 2% (v/v) DMSO. Compounds (10 mM stocks in 100% DMSO) were diluted in DMSO to 500 μM (DCLK1-NEG) or 25 μM (all other compounds) then in running buffer (without DMSO) to achieve the starting conentration with a final DMSO concentration of 2% (v/v). Samples were then serially titrated in running buffer containing 2% (v/v) DMSO to prepare each final concentration series (7-point, 3-fold serial dilution, 10 μM to 13.7 nM for DCLK1-NEG, or 500 nM to 0.68 nM for all other compounds). Solutions were injected in multi-cycle format (in duplicate) without regeneration (contact time 80 sec, flow rate 75 μL/min, dissociation time 600 sec), with an extra wash (50% DMSO) after each injection.

Data analysis. Steady state/kinetic binding data were fitted using the S200 BIAevaluation software (GE Healthcare). Sensorgrams from reference surfaces and blank injections were subtracted from the raw data (double-referencing), followed by solvent correction. Kinetic rate constants (k_{on} and k_{off} values) were obtained by fitting to 1:1 Langmuir binding model. Reported binding data represent mean ± SEM for three or four independent experiments. The dissociative half-life life ($t_{1/2}$) for each inhibitor complex with DCLK1 was calculated from the fitted dissociation rate constant (k_{off}), according the equation $t_{1/2} = \ln 2/k_{off.}$

Phos-Tag gels

Phos-tag™ pre-cast gel anaylsis of phosphorylated and non-phophorylated samples was done according to manufacturer's instruction (FUJIFILM Wako Pure Chemical Corporation). DCLK1 WT, DCLK1 WT treated with lamda phosphatase and DCLK1 D511N at 1 μg or 0.5 μg were run on a SuperSep™ Phos-tag™ 12.5% SDS-PAGE pre-cast gel. Electrophoresis was carried out at 150 volts for 60 min. The gel was stained using InstantBlue® Coomassie Protein Stain (Expedeon). A concevtional 12.5% SDS-PAGE analysis with molecular weight markers was done in parallel to ensure the proteins for the phos-tag analysis were not degraded.

Tubulin Polymerization and Pelleting Assay

Tubulin polymerization assays were performed in buffer containing 80 mM PIPES at pH 6.9, 2.0 mM $MgCl_2$, 0.5 mM EGTA, 2.5 mM β,γ-Methyleneguanosine 5′-triphosphate, and 10 μM tubulin and 5 μM DCLK1 for one hour at 37°C. For tubulin polymerisation in the presence of inhibitors, various concentrations of the inhibitors were first incubated with DCLK1 and allowed to stand on ice for 5min before adding this mix to the tubulin polymerisation reaction. Following the tubulin polymerisation, the reaction mix was pelleted at 20,000 g for 20min and the supernatant and the pellet

fractions were run on a 12% SDS gel. The data shown are representative of two independent experiments.

Tubulin polymerisation assay

Tubulin polymerisation assay were performed using the Microtubule Polymerisation/Depolymerisation Fluorescence Kit (Cytoskeleton #BK011P) in accordance with the manufcaturer's instructions. DCLK1 (4 μM) were added to 50 μL tubulin reaction mix containing Buffer 1 (80 mM PIPES at pH 6.9, 2.0 mM $MgCl_2$, 0.5 mM EGTA, 10 μM fluorescent reporter), guanosine triphosphate stock solution at 100 mM, and 10 mg/mL tubulin stock solution, using rations as described by the manufacturer. Paclitaxel, a control of tubulin polymerisation was tested at 3 μM and Nocodazole, a tubulin polymerisation inhibitor was tested at 80 μM. DCLK1-IN-1 was tested at 20 and 40 μM with DMSO and buffer alone as controls. Polymerisation is followed by fluorescence enhancement due to incorporation of a fluorescence reporter into microtubules as polymerisation occurs and was measured by excitation at 355 nm and emission at 460 nM. Readings were taken every 20 sec on EnVision Multimode Plate Reader. Each condition was tested in duplicates with two independent batch of proteins.

Data availability

Coordinates and structure factors of the structures of DCLK1-KD:XMD8-85, DCLK1-KD:FMF-03-055-1 and DCLK1-KD:DCLK1-IN-1 have been submitted in the Protein Data Bank with the following accession codes: PDB:7KX6, 7KX8 and 7KXW respectively.

The authors declare that all other data supporting the findings of this study are available within the article and its Supplementary Data files, or from the corresponding authors on request.

Acknowledgments

O.P was supported by an ARC Future Fellowship (FT120100056). I.L acknowledges the support from the Walter and Eliza Hall Institute. We are also grateful to the National Health and Medical Research Council for Grant support (APP1162058) with additional support from the Operational Infrastructure Support Program provided by the Victorian Government, Australia and from the Australian Cancer Research Foundation (to I.L, W.D, O.P, A.K, M.R). We acknowledge Melbourne Research Scholarship support for A.K. from the University of Melbourne. We would like to thank the staff at the Bio21 C3 Collaborative Crystallization Centre where all initial crystallisation experiments were performed and the beamline staff at the Australian Synchrotron where diffraction data were collected. We would also like to thank Nathanael Gray and Fleur Ferguson for providing the DCLK1 compounds.

Authors contributions

Conceptualization O.P, M.R, I.L; Methodology W.D, A.K, M.R, O.P; Investigation W.D, A.K, M.R, O.P; Writing original to final draft O.P, M.R and I.L with input from A.K. and W.D.; Review and editing O.P, M.R, I.L; Funding acquisition I.L, O.P; Project administration and supervision I.L, O.P.

Competing financial interests

The authors declare no competing financial interests.

References

1. May, R. et al. Identification of a novel putative gastrointestinal stem cell and adenoma stem cell marker, doublecortin and CaM kinase-like-1, following radiation injury and in adenomatous polyposis coli/multiple intestinal neoplasia mice. *Stem Cells* **26**, 630-7 (2008).
2. May, R. et al. Doublecortin and CaM kinase-like-1 and leucine-rich-repeat-containing G-protein-coupled receptor mark quiescent and cycling intestinal stem cells, respectively. *Stem Cells* **27**, 2571-9 (2009).
3. May, R. et al. Identification of a novel putative pancreatic stem/progenitor cell marker DCAMKL-1 in normal mouse pancreas. *Am J Physiol Gastrointest Liver Physiol* **299**, G303-10 (2010).
4. Bhat, K.M. & Setaluri, V. Microtubule-associated proteins as targets in cancer chemotherapy. *Clin Cancer Res* **13**, 2849-54 (2007).
5. Ramkumar, A., Sivakumar, N., Gujarathi, A.M. & Victor, R. Production of thermotolerant, detergent stable alkaline protease using the gut waste of Sardinella longiceps as a substrate: Optimization and characterization. *Sci Rep* **8**, 12442 (2018).
6. Gao, T. et al. DCLK1 is up-regulated and associated with metastasis and prognosis in colorectal cancer. *J Cancer Res Clin Oncol* **142**, 2131-40 (2016).
7. Ikezono, Y.U. et al. High expression of the putative cancer stem cell marker, DCLK1, in rectal neuroendocrine tumors. *Oncol Lett* **10**, 2015-2020 (2015).
8. Singh, P., O'Connell, M. & Shubhashish, S. Epigenetic regulation of human DCLK-1 gene during colon-carcinogenesis: clinical and mechanistic implications. *Stem Cell Investig* **3**, 51 (2016).
9. Sureban, S.M. et al. DCAMKL-1 regulates epithelial-mesenchymal transition in human pancreatic cells through a miR-200a-dependent mechanism. *Cancer Res* **71**, 2328-38 (2011).
10. Weygant, N. et al. DCLK1 is a broadly dysregulated target against epithelial-mesenchymal transition, focal adhesion, and stemness in clear cell renal carcinoma. *Oncotarget* **6**, 2193-205 (2015).
11. Cancer Genome Atlas Research, N. Comprehensive molecular characterization of gastric adenocarcinoma. *Nature* **513**, 202-9 (2014).
12. Wang, K. et al. Whole-genome sequencing and comprehensive molecular profiling identify new driver mutations in gastric cancer. *Nat Genet* **46**, 573-82 (2014).
13. Engels, B.M., Schouten, T.G., van Dullemen, J., Gosens, I. & Vreugdenhil, E. Functional differences between two DCLK splice variants. *Brain Res Mol Brain Res* **120**, 103-14 (2004).
14. Omori, Y. et al. Expression and chromosomal localization of KIAA0369, a putative kinase structurally related to Doublecortin. *J Hum Genet* **43**, 169-77 (1998).
15. Vreugdenhil, E. et al. Doublecortin-like, a microtubule-associated protein expressed in radial glia, is crucial for neuronal precursor division and radial process stability. *Eur J Neurosci* **25**, 635-48 (2007).
16. Burgess, H.A. & Reiner, O. Alternative splice variants of doublecortin-like kinase are differentially expressed and have different kinase activities. *J Biol Chem* **277**, 17696-705 (2002).
17. O'Connell, M.R. et al. Epigenetic changes and alternate promoter usage by human colon cancers for expressing DCLK1-isoforms: Clinical Implications. *Sci Rep* **5**, 14983 (2015).
18. Sarkar, S. et al. A novel antibody against cancer stem cell biomarker, DCLK1-S, is potentially useful for assessing colon cancer risk after screening colonoscopy. *Lab Invest* **97**, 1245-1261 (2017).
19. Vedeld, H.M., Skotheim, R.I., Lothe, R.A. & Lind, G.E. The recently suggested intestinal cancer stem cell marker DCLK1 is an epigenetic biomarker for colorectal cancer. *Epigenetics* **9**, 346-50 (2014).
20. Burgess, H.A. & Reiner, O. Cleavage of doublecortin-like kinase by calpain releases an active kinase fragment from a microtubule anchorage domain. *J Biol Chem* **276**, 36397-403 (2001).

21. Nagamine, T., Nomada, S., Onouchi, T., Kameshita, I. & Sueyoshi, N. Nuclear translocation of doublecortin-like protein kinase and phosphorylation of a transcription factor JDP2. *Biochem Biophys Res Commun* **446**, 73-8 (2014).
22. Sureban, S.M. et al. Plasma DCLK1 is a marker of hepatocellular carcinoma (HCC): Targeting DCLK1 prevents HCC tumor xenograft growth via a microRNA-dependent mechanism. *Oncotarget* **6**, 37200-15 (2015).
23. Sureban, S.M. et al. Selective blockade of DCAMKL-1 results in tumor growth arrest by a Let-7a MicroRNA-dependent mechanism. *Gastroenterology* **137**, 649-59, 659 e1-2 (2009).
24. Verissimo, C.S. et al. Silencing of the microtubule-associated proteins doublecortin-like and doublecortin-like kinase-long induces apoptosis in neuroblastoma cells. *Endocr Relat Cancer* **17**, 399-414 (2010).
25. Patel, O. et al. Biochemical and Structural Insights into Doublecortin-like Kinase Domain 1. *Structure* **24**, 1550-61 (2016).
26. Sureban, S.M. et al. XMD8-92 inhibits pancreatic tumor xenograft growth via a DCLK1-dependent mechanism. *Cancer Lett* **351**, 151-61 (2014).
27. Weygant, N. et al. Small molecule kinase inhibitor LRRK2-IN-1 demonstrates potent activity against colorectal and pancreatic cancer through inhibition of doublecortin-like kinase 1. *Molecular cancer* **13**, 103 (2014).
28. Ferguson, F.M. et al. Synthesis and Structure-Activity Relationships of DCLK1 Kinase Inhibitors Based on a 5,11-Dihydro-6H-benzo[e]pyrimido[5,4-b][1,4]diazepin-6-one Scaffold. *J Med Chem* **63**, 7817-7826 (2020).
29. Deng, X. et al. Characterization of a selective inhibitor of the Parkinson's disease kinase LRRK2. *Nat Chem Biol* **7**, 203-5 (2011).
30. Deng, X. et al. Discovery of a benzo[e]pyrimido-[5,4-b][1,4]diazepin-6(11H)-one as a Potent and Selective Inhibitor of Big MAP Kinase 1. *ACS Med Chem Lett* **2**, 195-200 (2011).
31. Ferguson, F.M. et al. Characterization of a highly selective inhibitor of the Aurora kinases. *Bioorg Med Chem Lett* **27**, 4405-4408 (2017).
32. Ferguson, F.M. et al. Discovery of a Series of 5,11-Dihydro-6H-benzo[e]pyrimido[5,4-b][1,4]diazepin-6-ones as Selective PI3K-delta/gamma Inhibitors. *ACS Med Chem Lett* **7**, 908-912 (2016).
33. Elkins, J.M. et al. X-ray crystal structure of ERK5 (MAPK7) in complex with a specific inhibitor. *J Med Chem* **56**, 4413-21 (2013).
34. Chen, H. et al. Discovery of a novel allosteric inhibitor-binding site in ERK5: comparison with the canonical kinase hinge ATP-binding site. *Acta Crystallogr D Struct Biol* **72**, 682-93 (2016).
35. Deng, X. et al. Structural determinants for ERK5 (MAPK7) and leucine rich repeat kinase 2 activities of benzo[e]pyrimido-[5,4-b]diazepine-6(11H)-ones. *Eur J Med Chem* **70**, 758-67 (2013).
36. Miduturu, C.V. et al. High-throughput kinase profiling: a more efficient approach toward the discovery of new kinase inhibitors. *Chem Biol* **18**, 868-79 (2011).
37. Ferguson, F.M. et al. Discovery of a selective inhibitor of doublecortin like kinase 1. *Nat Chem Biol* **16**, 635-643 (2020).
38. Gilsbach, B.K. et al. Structural Characterization of LRRK2 Inhibitors. *J Med Chem* **58**, 3751-6 (2015).
39. Panneerselvam, J. et al. DCLK1 Regulates Tumor Stemness and Cisplatin Resistance in Non-small Cell Lung Cancer via ABCD-Member-4. *Mol Ther Oncolytics* **18**, 24-36 (2020).
40. Sakaguchi, M. et al. miR-137 Regulates the Tumorigenicity of Colon Cancer Stem Cells through the Inhibition of DCLK1. *Mol Cancer Res* (2016).
41. Sureban, S.M. et al. DCLK1 regulates pluripotency and angiogenic factors via microRNA-dependent mechanisms in pancreatic cancer. *PLoS One* **8**, e73940 (2013).
42. Hammond, D.E. et al. Differential reprogramming of isogenic colorectal cancer cells by distinct activating KRAS mutations. *J Proteome Res* **14**, 1535-46 (2015).

43. Ge, Y. et al. Alternative splice variants of DCLK1 mark cancer stem cells, promote self-renewal and drug-resistance, and can be targeted to inhibit tumorigenesis in kidney cancer. *Int J Cancer* **143**, 1162-1175 (2018).
44. Qu, D. et al. Doublecortin-like kinase 1 is elevated serologically in pancreatic ductal adenocarcinoma and widely expressed on circulating tumor cells. *PLoS One* **10**, e0118933 (2015).
45. Murphy, J.M. et al. A robust methodology to subclassify pseudokinases based on their nucleotide-binding properties. *Biochem J* **457**, 323-34 (2014).
46. Lin, P.T., Gleeson, J.G., Corbo, J.C., Flanagan, L. & Walsh, C.A. DCAMKL1 encodes a protein kinase with homology to doublecortin that regulates microtubule polymerization. *J Neurosci* **20**, 9152-61 (2000).
47. Wang, Y. et al. Structures of a diverse set of colchicine binding site inhibitors in complex with tubulin provide a rationale for drug discovery. *FEBS J* **283**, 102-11 (2016).
48. Guimaraes, C.R. et al. Understanding the impact of the P-loop conformation on kinase selectivity. *J Chem Inf Model* **51**, 1199-204 (2011).
49. Liu, Y. et al. Chemical Biology Toolkit for DCLK1 Reveals Connection to RNA Processing. *Cell Chem Biol* (2020).
50. Nagamine, T., Shimomura, S., Sueyoshi, N. & Kameshita, I. Influence of Ser/Pro-rich domain and kinase domain of double cortin-like protein kinase on microtubule-binding activity. *J Biochem* **149**, 619-27 (2011).
51. Brugg, B. & Matus, A. Phosphorylation determines the binding of microtubule-associated protein 2 (MAP2) to microtubules in living cells. *J Cell Biol* **114**, 735-43 (1991).
52. Ramkumar, A., Jong, B.Y. & Ori-McKenney, K.M. ReMAPping the microtubule landscape: How phosphorylation dictates the activities of microtubule-associated proteins. *Dev Dyn* **247**, 138-155 (2018).
53. Toriyama, M. et al. Phosphorylation of doublecortin by protein kinase A orchestrates microtubule and actin dynamics to promote neuronal progenitor cell migration. *J Biol Chem* **287**, 12691-702 (2012).
54. Winter, G.E. et al. DRUG DEVELOPMENT. Phthalimide conjugation as a strategy for in vivo target protein degradation. *Science* **348**, 1376-81 (2015).
55. Bondeson, D.P. et al. Catalytic in vivo protein knockdown by small-molecule PROTACs. *Nat Chem Biol* **11**, 611-7 (2015).
56. Kabsch, W. Integration, scaling, space-group assignment and post-refinement. *Acta Crystallogr D Biol Crystallogr* **66**, 133-44 (2010).
57. Kabsch, W. Xds. *Acta Crystallogr D Biol Crystallogr* **66**, 125-32 (2010).
58. Afonine, P.V. et al. Towards automated crystallographic structure refinement with phenix.refine. *Acta Crystallogr D Biol Crystallogr* **68**, 352-67 (2012).
59. Emsley, P. & Cowtan, K. Coot: model-building tools for molecular graphics. *Acta Crystallogr D Biol Crystallogr* **60**, 2126-32 (2004).

Table 1. Human DCLK1 isoforms in cancer

Human DCLK1 isoforms	Cancer	Reference
DCLK1-L, DCL	Neuroblastic tumors, Neuroblastoma cell lines	39
DCLK1-S	Colorectal cancer cell line (SW48) harbouring codon K12 KRAS mutations	40
DCLK1-S (NM_001195415.1)	Colon adenocarcinomas, Colon cancer cell lines (LOVO, SW1116, SW837, SW948, HCT116, SW-480, DLD1, RKO, LS411N, HT29, NCIH508, Caco2, COLO320)	17
DCLK1-S	Non-small cell lung cancer (NSCLC) (cell line H460 and A549)	36
DCLK1-L	Non-small cell lung cancer (NSCLC) (cell line H1299)	
DCLK1-L (DCLK1-short-α; UniProtKB: O15075-2; ENST00000255448.8)	Renal clear cell carcinoma	41
DCLK1-L (DCLK1-long-α; UniProtKB: O15075-1; ENST00000360631.7)		
DCLK1-S (DCLK1-long-β UniProtKB: O15075-4; ENST00000379893.5)		
DCLK1-L	Serum samples from patients with Pancreatic ductal adenocarcinoma	42
DCLK1-S (Uniport isoform O15075-3, -4)	Pancreatic ductal adenocarcinoma cell lines PATU-8988T, PATU-8902	34
DCLK1-S (Uniport isoform O15075-3, -4)	Pancreatic ductal adenocarcinoma organoids PANFR0029_T2, PANFR0172_T2, PANFR0172_T3, PANFR0172_T4	34

FIGURE LEGENDS

Fig. 1. Benzopyrimido-diazipinone scaffolds and their binding to DCLK1-KD. **a** Top, DCLK1 domain architecture highlighting the DCX domains at the N-terminal region and the kinase domain with its C-terminal regulatory tail (CT) at the C-terminal region. The N-terminal and the C-terminal regions are connected by the serine/proline (S/P) rich linker. Bottom, Chemical structures of benzopyrimido-diazipinone scaffolds. R1, R2, R3 and R4 positions previously described[28] are labelled. **b** The difference in melting temperature of DCLK1-KD against the concentration of XMD8-85, DCLK1-IN-1 and DCLK1-NEG. The difference in the Tm was calculated from the melting profiles shown in Figure S1.

Fig. 2. Structure of DCLK1-KD:XMD8-85. **a** The structure of two molecules of DCLK1-KD:XMD8-85 within the asymmetric unit in a "head-to-tail" arrangement. **b** The structure of two molecules of DCLK1-KD:AMP-PN (PDB 5JZJ) within the asymmetric unit in a "head-to-tail" and "face-to-face" arrangement. **c** Overlay of DCLK1-KD:XMD8-85 with DCLK1-KD:NVP-TAE684 showing the conservation of the canonical salt-bridge between Glu436 and Lys419 and differences in the αC helix conformation. **d** Top view of the overlay of DCLK1-KD:XMD8-85 with DCLK1-KD:NVP-TAE684. XMD8-85, rings B and A sits deeper into the back pocket within the ATP binding site. **e** Close up of the interaction of DCLK1-KD with XMD-8-85. **f** Water mediated network formed by the diazepine ring B with the invariant Lys419 and Glu436. **g** Surface representation of DCLK1-KD:XMD8-85 to highlight the cavity around the water mediated network described in **e**. **h** The DCLK1-KD:XMD8-85 crystal structure identified two cavities near the back pocket within the ATP binding site that could be exploited to achieve selectivity towards DCLK1. The h-bond and van der Waals interaction are shown in black and red dashed lines, respectively. The tip of the glycine loop with missing residues in DCLK1-KD:XMD8-85 is shown in pink dashed lines. Water molecules are shown as blue spheres. XMD8-85, yellow; NVP-TAE684, cyan.

Fig. 3. Structure of DCLK1-Cter:FMF-03-055-1. **a** The structure of two molecules of DCLK1-Cter:FMF-03-055-1 within the asymmetric unit in a "head-to-tail" arrangement. **b** Close up of the interaction of DCLK1-KD with FMF-03-055-1. **c** Top, overlay of DCLK1-Cter:FMF-03-055-1with ERK5:XMD8-92 showing the differences in the gatekeeper residues, Leu137 in ERK5 and Met 465 in DCLK1. Bottom, ligand interaction diagrams generated using Schrödinger Maestro, including prediction of protonation states at pH 7.0 using Epik (Release 2020-3:, Schrödinger, LLC, New York, NY, 2020). **d** Surface representation of DCLK1-Cter:FMF-03-055-1 and ERK5:XMD8-92 to

highlight the collapsed N-lobe towards the C-lobe. The h-bond and van der Waals interaction are shown in black and red dashed lines, respectively. FMF-03-055-1, magenta; XMD8-92, teal.

Fig. 4. Structure of DCLK1-KD:DCLK1-IN-1. **a** The structure of two molecules of DCLK1-KD:DCLK1-IN-1 within the asymmetric unit in a "head-to-tail" arrangement. **b** Close up of the interaction of DCLK1-KD with DCLK1-IN-1. **c** Top, overlay of DCLK1-Cter:FMF-03-055-1 with DCLK1-KD:DCLK1-IN-1 to highlight the opening of the ATP binding site. The glycine loop and the β3 strand undergoing a significant upward shift (shown with arrows) to accommodate the bulky trifluoroethyl group. Bottom, DCLK1-KD:DCLK1-IN-1 showing the allosteric pocket occupied by a PEG molecule. **d** Top, surface representation of DCLK1-KD:XMD8-85, DCLK1-Cter:FMF-03-055-1 and DCLK1-KD:DCLK1-IN-1 to show the differences in the ATP binding sites and conformational changes. Bottom, ligand interaction diagrams generated using Schrödinger Maestro as described in Fig. 2. The h-bond and van der Waals interaction are shown in black and red dashed lines, respectively. DCLK1-IN-1, purple; FMF-03-055-1, magenta. See also Figure S4.

Fig. 5. DCLK1 isoforms and the effect of DCLK1-IN-1 on microtubule polymerisation and binding function. **a** DCLK1 isoforms based on the Uniprot classification. **b** The difference in melting temperature of DCLK1-KD, DCLK1-FL1Δ D511N and DCLK1-WT with binding to DCLK1-IN-1 and DCLK1-NEG. The difference in the Tm was calculated from the melting profiles shown in Figure S5. **c** Representative fitted SPR sensorgrams for DCLK1-IN-1, FMF-03-055-1 or XMD8-85 binding to immobilised DCLK1-FL1Δ D511N, showing mean values from kinetic fitting to a 1:1 binding model (K_D, dissociation constant; k_{on}, on-rate; k_{off}, off-rate; $t_{1/2}$, dissociative half-life for the protein/inhibitor complex). Data represents an average of either four (DCLK1-IN-1) or three (FMF-03-0550-1 and XMD8-85) independent experiments, each performed as duplicate titrations; errors are SEM. See also Figure S6. **d** SDS-PAGE gel analysis of pellet and supernatant fractions following tubulin polymerisation in the presence of DCLK1-FL1Δ D511N. Tubulin was incubated with a control buffer, DCLK1-FL1Δ D511N, paclitaxel, DCLK1-IN-1, nocodazol and DMSO. This curve is a representation of samples tested in duplicates and in two independent experiments. See also Figure S8. **e**. Tubulin polymerisation assay. Tubulin was incubated with a control buffer, DCLK1-FL1Δ D511N, paclitaxel, DCLK1-IN-1, nocodazol and DMSO. This curve is a representation of samples tested in duplicates and in two independent experiments. See also Figure S7.

a

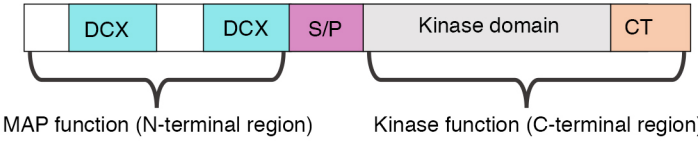

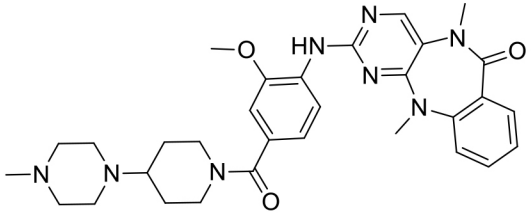
LRRK2-IN-1

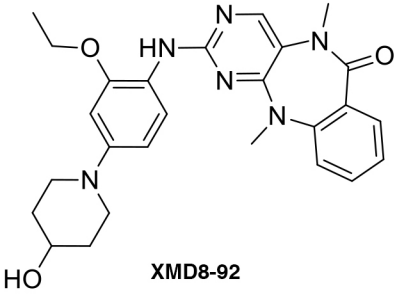
XMD8-92

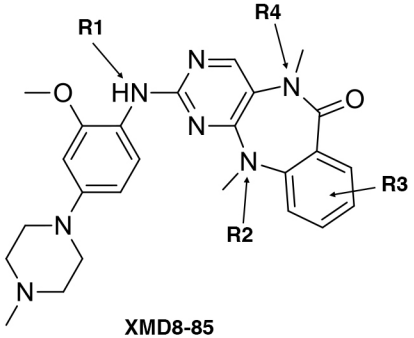

XMD8-85

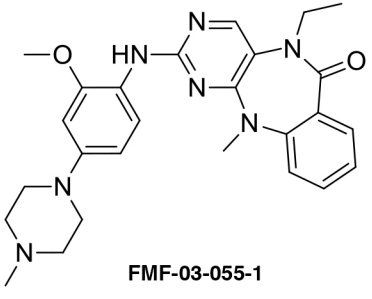
FMF-03-055-1

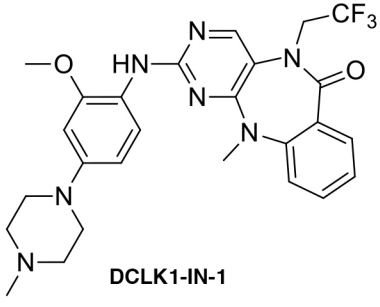
DCLK1-IN-1

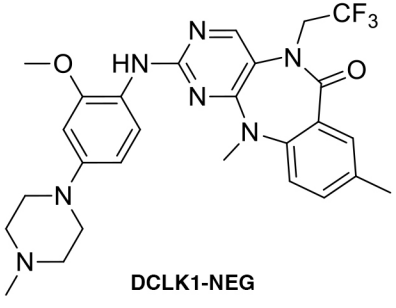
DCLK1-NEG

b

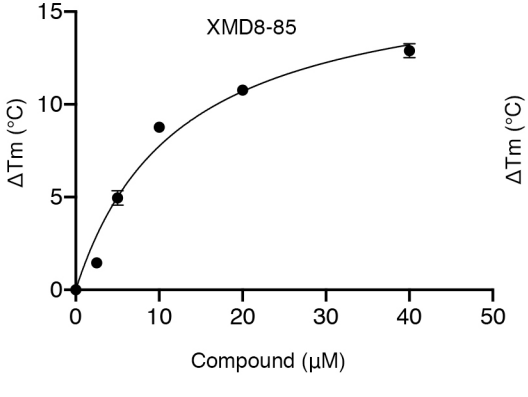

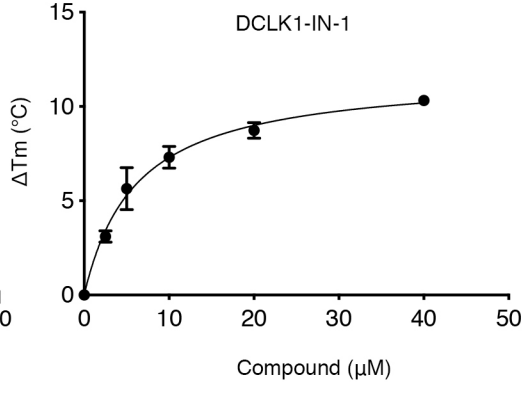

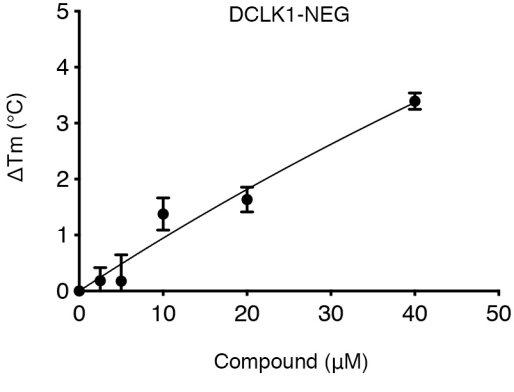

Fig. 2

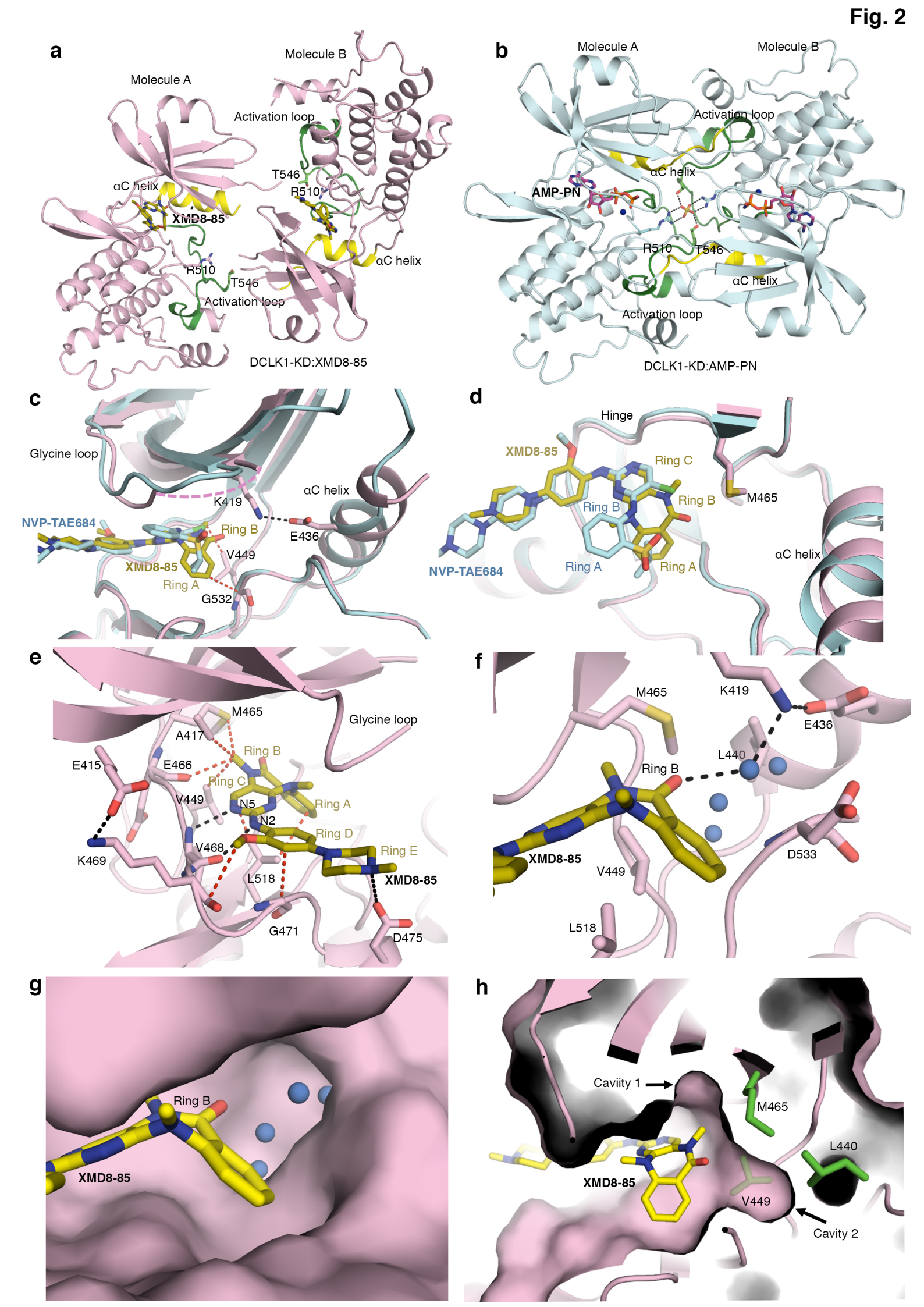
a
Molecule A
Molecule B
Activation loop
αC helix
T546
R510
XMD8-85
αC helix
R510
T546
Activation loop
DCLK1-KD:XMD8-85
b
Molecule A
Molecule B
Activation loop
αC helix
AMP-PN
R510
T546
αC helix
Activation loop
DCLK1-KD:AMP-PN
c
Glycine loop
αC helix
K419
NVP-TAE684
Ring B
E436
V449
XMD8-85
Ring A
G532
d
Hinge
XMD8-85
Ring C
Ring B
Ring B
M465
NVP-TAE684
Ring A
Ring A
αC helix
e
M465
Glycine loop
A417
Ring B
E415
E466
Ring C
V449
N5
Ring A
N2
Ring D
V468
Ring E
K469
L518
XMD8-85
G471
D475
f
M465
K419
E436
L440
Ring B
XMD8-85
V449
D533
L518
g
Ring B
XMD8-85
h
Caviity 1
M465
L440
XMD8-85
V449
Cavity 2

Fig. 3

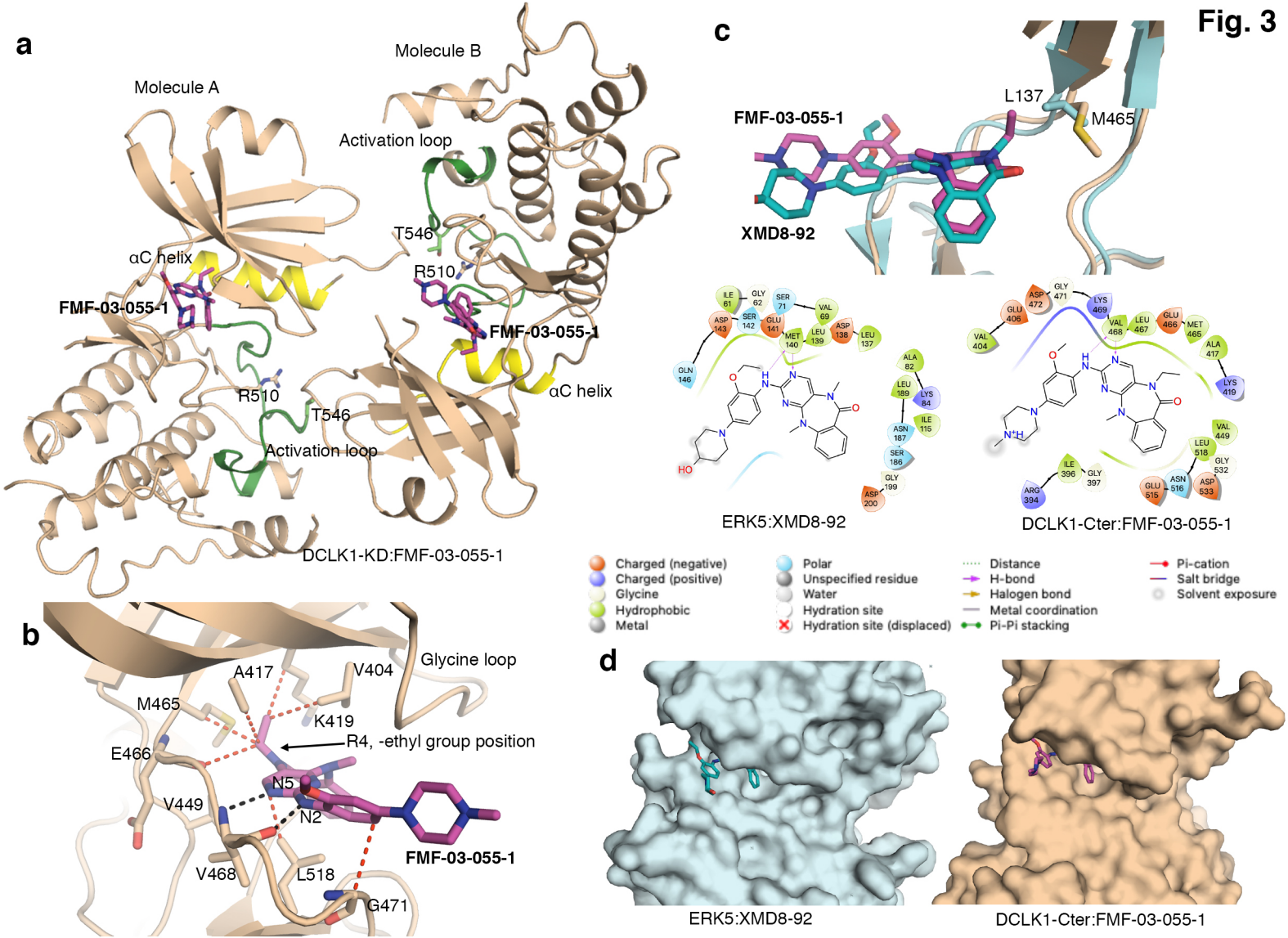
a
Molecule A
Molecule B
Activation loop
αC helix
FMF-03-055-1
T546
R510
FMF-03-055-1
αC helix
R510
T546
Activation loop
DCLK1-KD:FMF-03-055-1
b
Glycine loop
A417
V404
M465
K419
R4, -ethyl group position
E466
N5
V449
N2
FMF-03-055-1
V468
L518
G471
c
L137
M465
FMF-03-055-1
XMD8-92
ERK5:XMD8-92
DCLK1-Cter:FMF-03-055-1
Charged (negative)
Charged (positive)
Glycine
Hydrophobic
Metal
Polar
Unspecified residue
Water
Hydration site
Hydration site (displaced)
Distance
H-bond
Halogen bond
Metal coordination
Pi-Pi stacking
Pi-cation
Salt bridge
Solvent exposure
d
ERK5:XMD8-92
DCLK1-Cter:FMF-03-055-1

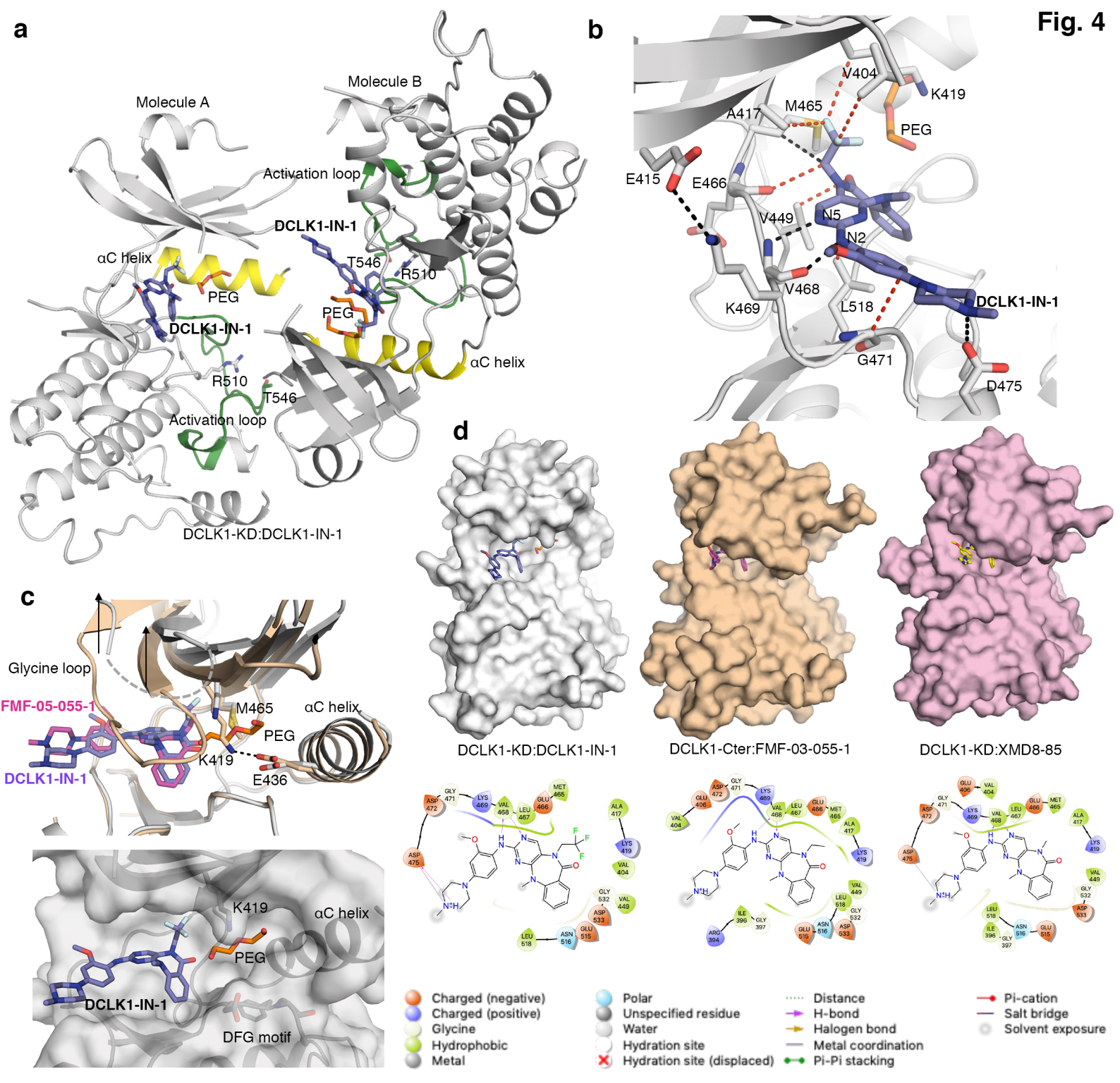
a
Molecule A
Molecule B
Activation loop
DCLK1-IN-1
αC helix
T546
R510
PEG
PEG
DCLK1-IN-1
αC helix
R510
T546
Activation loop
DCLK1-KD:DCLK1-IN-1
b
V404
K419
A417
M465
PEG
E415
E466
V449
N5
N2
V468
K469
L518
DCLK1-IN-1
G471
D475
c
Glycine loop
FMF-05-055-1
M465
αC helix
PEG
K419
DCLK1-IN-1
E436
K419
αC helix
PEG
DCLK1-IN-1
DFG motif
d
DCLK1-KD:DCLK1-IN-1
DCLK1-Cter:FMF-03-055-1
DCLK1-KD:XMD8-85
Charged (negative)
Charged (positive)
Glycine
Hydrophobic
Metal
Polar
Unspecified residue
Water
Hydration site
Hydration site (displaced)
Distance
H-bond
Halogen bond
Metal coordination
Pi-Pi stacking
Pi-cation
Salt bridge
Solvent exposure

Fig. 5

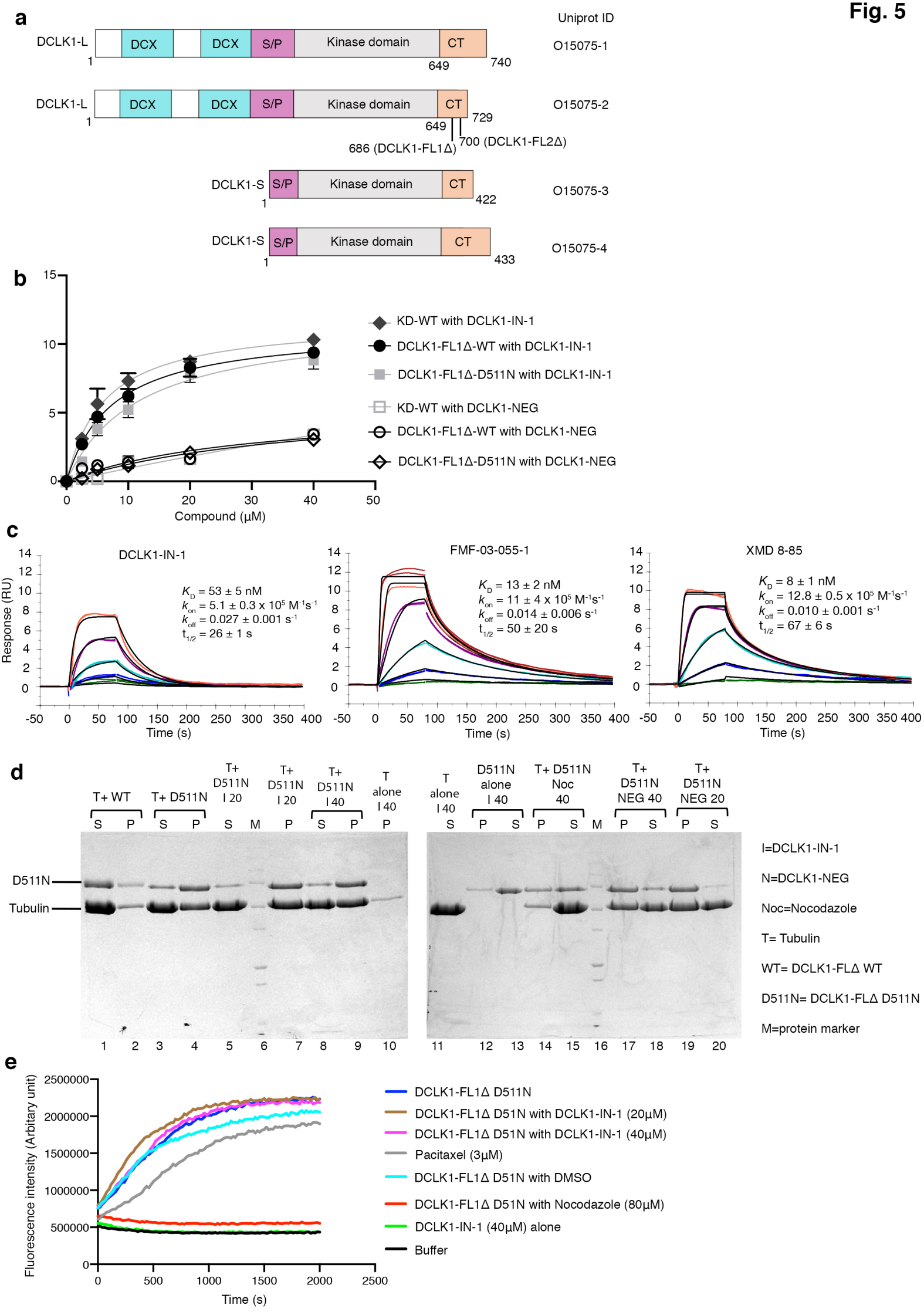
a
Uniprot ID
DCLK1-L
DCX
DCX
S/P
Kinase domain
CT
1
649
740
O15075-1
DCLK1-L
DCX
DCX
S/P
Kinase domain
CT
1
649
729
686 (DCLK1-FL1Δ)
700 (DCLK1-FL2Δ)
O15075-2
DCLK1-S
S/P
Kinase domain
CT
1
422
O15075-3
DCLK1-S
S/P
Kinase domain
CT
1
433
O15075-4
b
KD-WT with DCLK1-IN-1
DCLK1-FL1Δ-WT with DCLK1-IN-1
DCLK1-FL1Δ-D511N with DCLK1-IN-1
KD-WT with DCLK1-NEG
DCLK1-FL1Δ-WT with DCLK1-NEG
DCLK1-FL1Δ-D511N with DCLK1-NEG
Compound (μM)
c
DCLK1-IN-1
K_D = 53 ± 5 nM
k_{on} = 5.1 ± 0.3 x 10^5 $M^{-1}s^{-1}$
k_{off} = 0.027 ± 0.001 s^{-1}
$t_{1/2}$ = 26 ± 1 s
FMF-03-055-1
K_D = 13 ± 2 nM
k_{on} = 11 ± 4 x 10^5 $M^{-1}s^{-1}$
k_{off} = 0.014 ± 0.006 s^{-1}
$t_{1/2}$ = 50 ± 20 s
XMD 8-85
K_D = 8 ± 1 nM
k_{on} = 12.8 ± 0.5 x 10^5 $M^{-1}s^{-1}$
k_{off} = 0.010 ± 0.001 s^{-1}
$t_{1/2}$ = 67 ± 6 s
Response (RU)
Time (s)
d
T+ WT
T+ D511N
T+ D511N I 20
T+ D511N I 20
T+ D511N I 40
T alone I 40
T alone I 40
D511N alone I 40
T+ D511N Noc 40
T+ D511N NEG 40
T+ D511N NEG 20
S P S P S M P S P P S P S P M P S P S
D511N
Tubulin
1 2 3 4 5 6 7 8 9 10 11 12 13 14 15 16 17 18 19 20
I=DCLK1-IN-1
N=DCLK1-NEG
Noc=Nocodazole
T= Tubulin
WT= DCLK1-FLΔ WT
D511N= DCLK1-FLΔ D511N
M=protein marker
e
Fluorescence intensity (Arbitary unit)
Time (s)
DCLK1-FL1Δ D511N
DCLK1-FL1Δ D51N with DCLK1-IN-1 (20μM)
DCLK1-FL1Δ D51N with DCLK1-IN-1 (40μM)
Pacitaxel (3μM)
DCLK1-FL1Δ D51N with DMSO
DCLK1-FL1Δ D51N with Nocodazole (80μM)
DCLK1-IN-1 (40μM) alone
Buffer

Figures

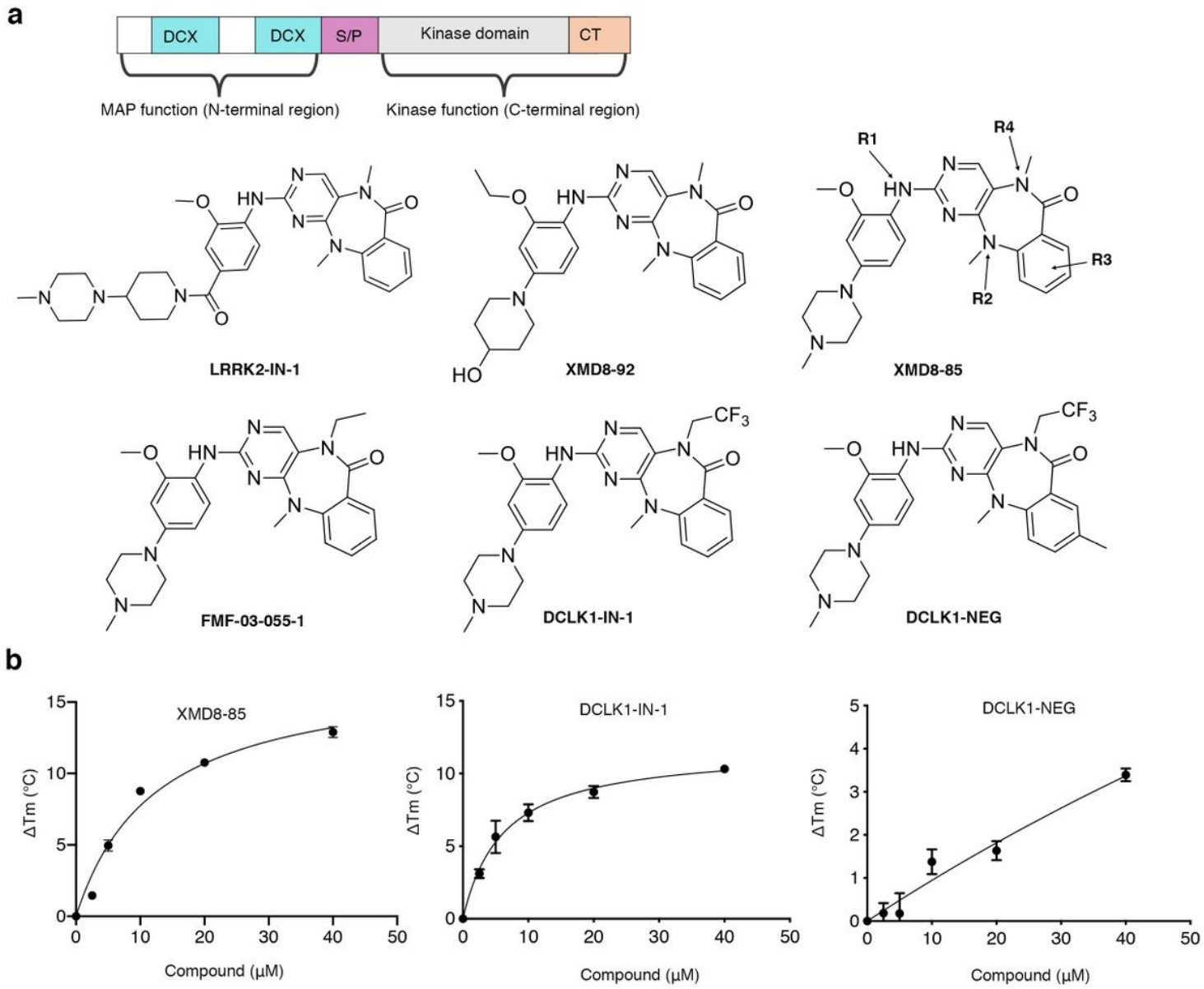

Figure 1

Benzopyrimido-diazipinone scaffolds and their binding to DCLK1-KD. a Top, DCLK1 domain architecture highlighting the DCX domains at the N-terminal region and the kinase domain with its C-terminal regulatory tail (CT) at the C-terminal region. The N-terminal and the C-terminal regions are connected by the serine/proline (S/P) rich linker. Bottom, Chemical structures of benzopyrimido-diazipinone scaffolds. R1, R2, R3 and R4 positions previously described28 are labelled. b The difference in melting temperature of DCLK1-KD against the concentration of XMD8-85, DCLK1-IN-1 and DCLK1-NEG. The difference in the Tm was calculated from the melting profiles shown in Figure S1.

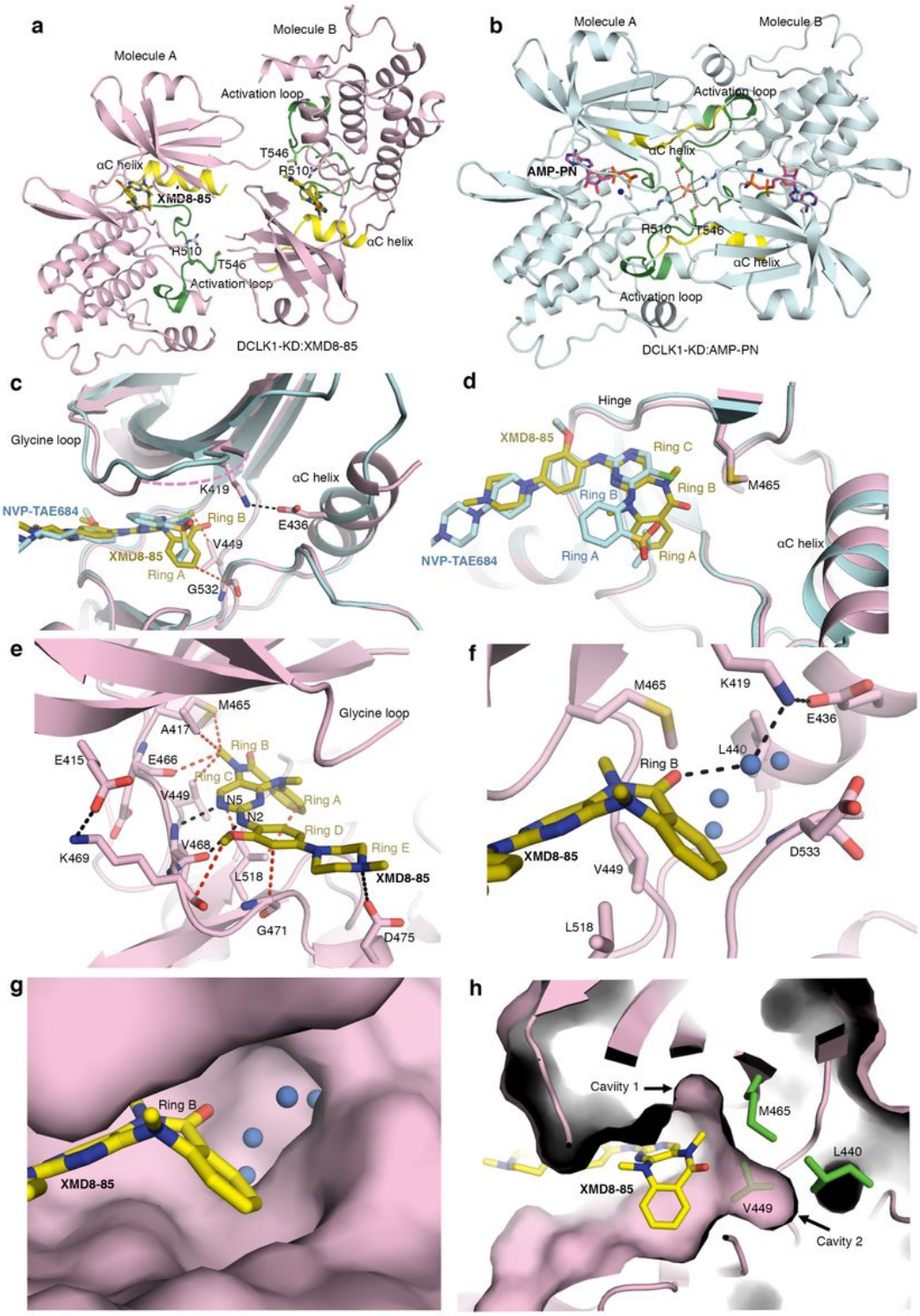

Figure 2

Structure of DCLK1-KD:XMD8-85. a The structure of two molecules of DCLK1-KD:XMD8-85 within the asymmetric unit in a “head-to-tail” arrangement. b The structure of two molecules of DCLK1-KD:AMP-PN (PDB 5JZJ) within the asymmetric unit in a “head-to-tail” and “face-to-face” arrangement. c Overlay of DCLK1-KD:XMD8-85 with DCLK1-KD:NVP-TAE684 showing the conservation of the canonical salt-bridge between Glu436 and Lys419 and differences in the aC helix conformation. d Top view of the overlay of

DCLK1-KD:XMD8-85 with DCLK1-KD:NVP-TAE684. XMD8-85, rings B and A sits deeper into the back pocket within the ATP binding site. e Close up of the interaction of DCLK1-KD with XMD-8-85. f Water mediated network formed by the diazepine ring B with the invariant Lys419 and Glu436. g Surface representation of DCLK1-KD:XMD8-85 to highlight the cavity around the water mediated network described in e. h The DCLK1-KD:XMD8-85 crystal structure identified two cavities near the back pocket within the ATP binding site that could be exploited to achieve selectivity towards DCLK1. The h-bond and van der Waals interaction are shown in black and red dashed lines, respectively. The tip of the glycine loop with missing residues in DCLK1-KD:XMD8-85 is shown in pink dashed lines. Water molecules are shown as blue spheres. XMD8-85, yellow; NVP-TAE684, cyan.

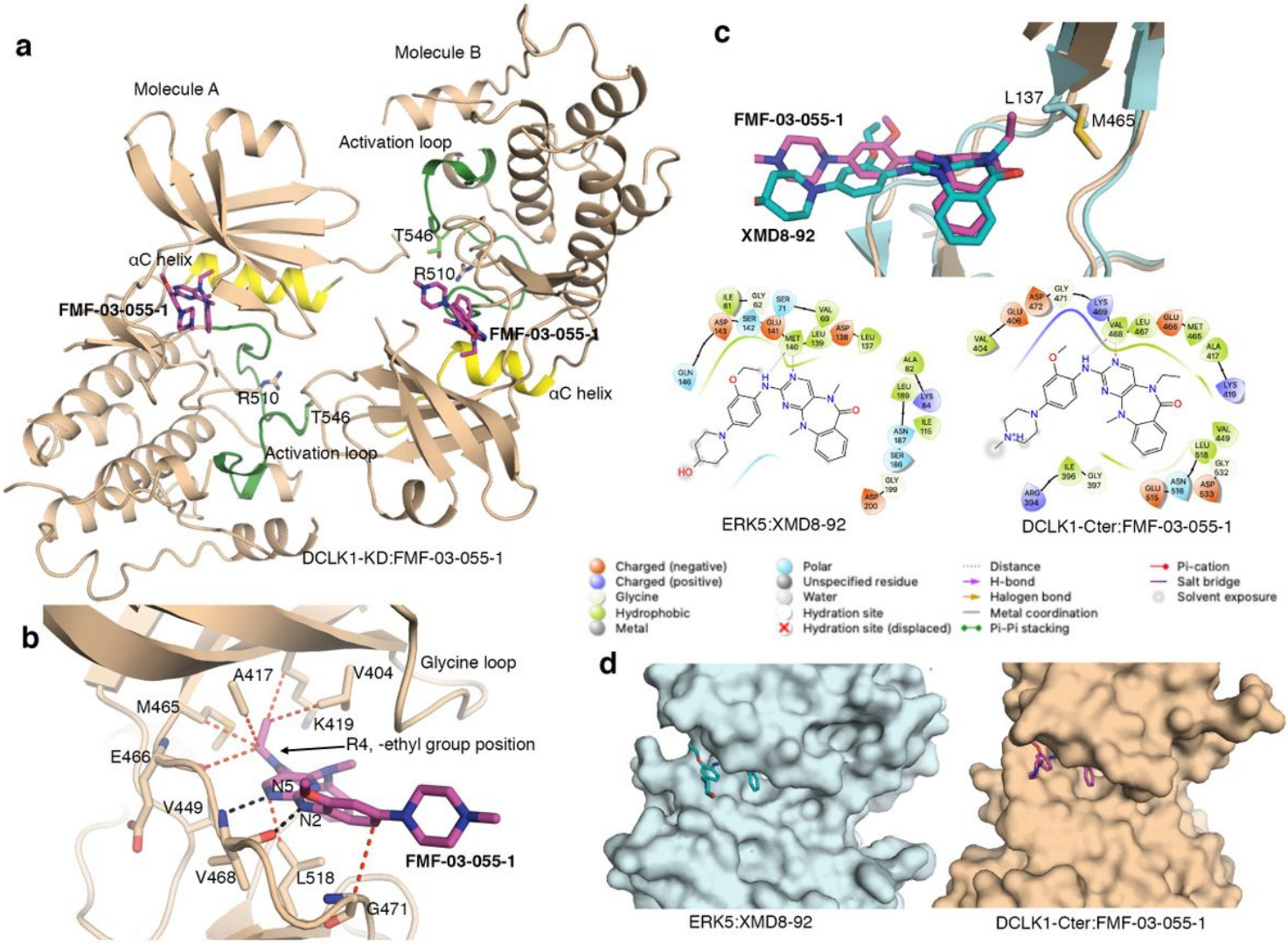

Figure 3

Structure of DCLK1-Cter:FMF-03-055-1. a The structure of two molecules of DCLK1-Cter:FMF-03-055-1 within the asymmetric unit in a “head-to-tail” arrangement. b Close up of the interaction of DCLK1-KD with FMF-03-055-1. c Top, overlay of DCLK1-Cter:FMF-03-055-1with ERK5:XMD8-92 showing the differences in the gatekeeper residues, Leu137 in ERK5 and Met 465 in DCLK1. Bottom, ligand interaction diagrams generated using Schrödinger Maestro, including prediction of protonation states at pH 7.0 using Epik (Release 2020-3:, Schrödinger, LLC, New York, NY, 2020). d Surface representation of DCLK1-

Cter:FMF-03-055-1 and ERK5:XMD8-92 to highlight the collapsed N-lobe towards the C-lobe. The h-bond and van der Waals interaction are shown in black and red dashed lines, respectively. FMF-03-055-1, magenta; XMD8-92, teal.

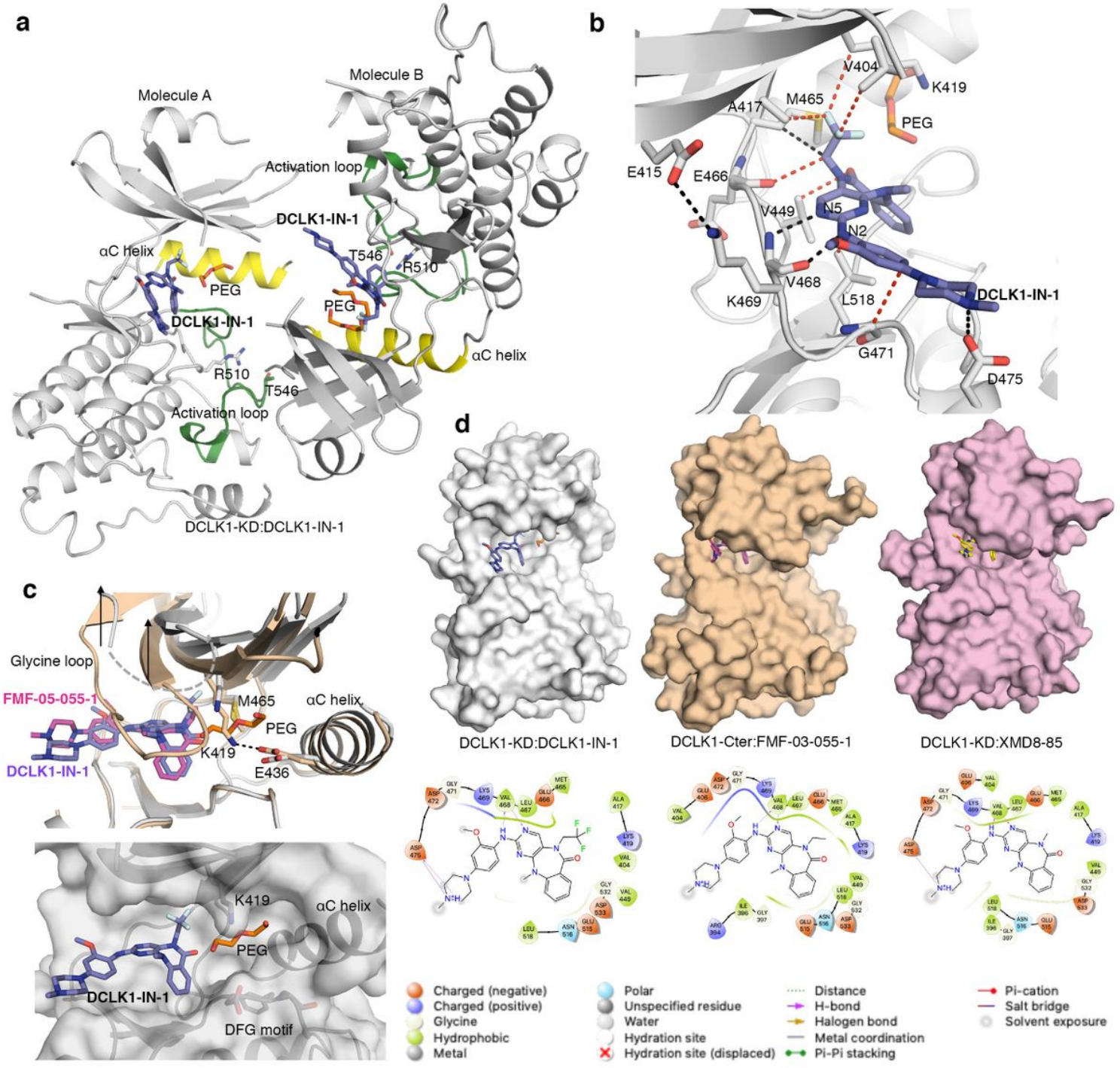

Figure 4

Structure of DCLK1-KD:DCLK1-IN-1. a The structure of two molecules of DCLK1-KD:DCLK1-IN-1 within the asymmetric unit in a “head-to-tail” arrangement. b Close up of the interaction of DCLK1-KD with DCLK1-IN-1. c Top, overlay of DCLK1-Cter:FMF-03-055-1 with DCLK1-KD:DCLK1-IN-1 to highlight the opening of the ATP binding site. The glycine loop and the b3 strand undergoing a significant upward shift (shown

with arrows) to accommodate the bulky trifluoroethyl group. Bottom, DCLK1-KD:DCLK1-IN-1 showing the allosteric pocket occupied by a PEG molecule. d Top, surface representation of DCLK1-KD:XMD8-85, DCLK1-Cter:FMF-03-055-1 and DCLK1-KD:DCLK1-IN-1 to show the differences in the ATP binding sites and conformational changes. Bottom, ligand interaction diagrams generated using Schrödinger Maestro as described in Fig. 2. The h-bond and van der Waals interaction are shown in black and red dashed lines, respectively. DCLK1-IN-1, purple; FMF-03-055-1, magenta. See also Figure S4.

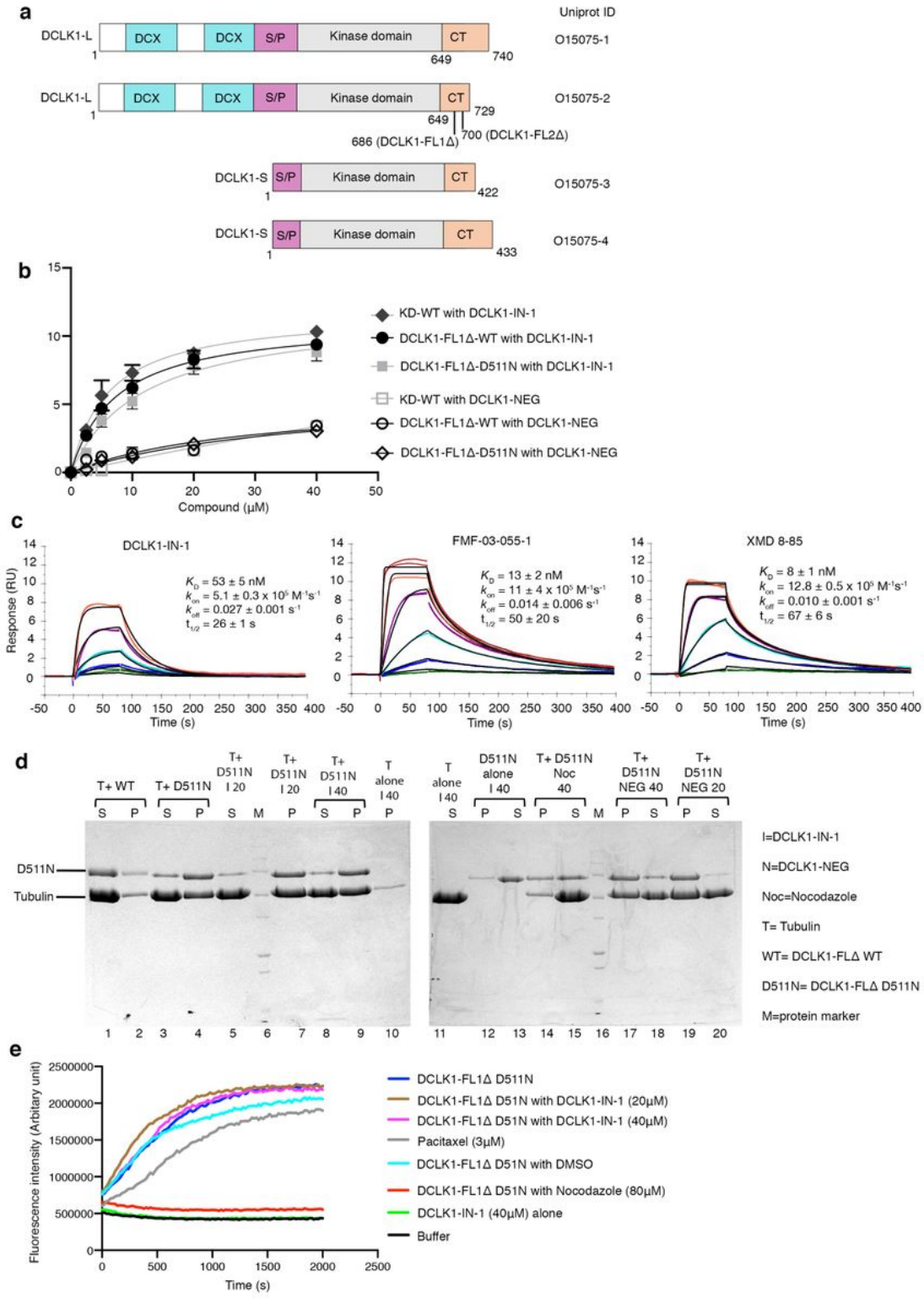

Figure 5

DCLK1 isoforms and the effect of DCLK1-IN-1 on microtubule polymerisation and binding function. a DCLK1 isoforms based on the Uniprot classification. b The difference in melting temperature of DCLK1-KD, DCLK1-FL1D D511N and DCLK1-WT with binding to DCLK1-IN-1 and DCLK1-NEG. The difference in the Tm was calculated from the melting profiles shown in Figure S5. c Representative fitted SPR sensorgrams for DCLK1-IN-1, FMF-03-055-1 or XMD8-85 binding to immobilised DCLK1-FL1D D511N, showing mean values from kinetic fitting to a 1:1 binding model (KD, dissociation constant; kon, on-rate; koff, off-rate; t1/2, dissociative half-life for the protein/inhibitor complex). Data represents an average of either four (DCLK1-IN-1) or three (FMF-03-0550-1 and XMD8-85) independent experiments, each performed as duplicate titrations; errors are SEM. See also Figure S6. d SDS-PAGE gel analysis of pellet and supernatant fractions following tubulin polymerisation in the presence of DCLK1-FL1D D511N. Tubulin was incubated with a control buffer, DCLK1-FL1D D511N, paclitaxel, DCLK1-IN-1, nocodazol and DMSO. This curve is a representation of samples tested in duplicates and in two independent experiments. See also Figure S8. e. Tubulin polymerisation assay. Tubulin was incubated with a control buffer, DCLK1-FL1D D511N, paclitaxel, DCLK1-IN-1, nocodazol and DMSO. This curve is a representation of samples tested in duplicates and in two independent experiments. See also Figure S7.

Supplementary Files

This is a list of supplementary files associated with this preprint. Click to download.

- PateletalSupplsection21122020.pdf
- FMF030551D1000253320valreportfullP1.pdf
- DCLK1IN1D1000253322valreportfullP1.pdf
- XMD885D1000253305valreportfullP1.pdf
- nrreportingsummaryPateletalfinal.pdf